Initial spindle positioning at the oocyte center protects against incorrect kinetochore-microtubule attachment and aneuploidy in mice

Jessica N. Kincade[1], Avery Hlavacek[1], Takashi Akera[2] and Ahmed Z. Balboula[1]*

[1] Animal Sciences Research Center, University of Missouri, Columbia, MO 65211, USA

[2]Cell and Developmental Biology Center, National Heart, Lung, and Blood Institute, National Institutes of Health, Bethesda, MD 20892, USA

Running title: Central spindle positioning protects against aneuploidy

Keywords: Aneuploidy, Nucleus Positioning, Spindle Positioning, Oocyte, Meiosis

*Corresponding author: Ahmed Z. Balboula, Animal Sciences Research Center, University of Missouri, Columbia, MO 65211, USA, abalboula@missouri.edu

ABSTRACT

Spindle positioning within the oocyte must be regulated tightly. Following nuclear envelope breakdown (NEBD), the spindle is predominantly assembled at the oocyte center prior to its migration towards the cortex to achieve the highly asymmetric division, a characteristic of female meiosis. The significance of the initial central positioning of the spindle is largely unknown. Here we show that the centered spindle in mouse oocytes is an insurance mechanism to avoid the premature exposure to cortical CDC42 signaling, which perturbs proper kinetochore-microtubule attachments, leading to the formation of aneuploid gametes. Because the spindle forms where NEBD occurs, nucleus position significantly influences the location of the initial spindle assembly. We also find that this nucleus positioning is a dynamic process that depends on maternal age. These findings will help in understanding why female gametes are notoriously associated with high rates of aneuploidy, the leading genetic cause of miscarriage and congenital abnormalities.

INTRODUCTION

Infertility is a globally prevalent issue affecting approximately 122 million women worldwide (*1*). Errors in chromosome segregation during meiosis result in aneuploidy, the leading genetic cause of miscarriage and congenital birth defects such as Down syndrome (*2, 3*). Aneuploidy occurs in females of all ages, but females of young age (9-20 years) and women of advanced age experience elevated risk of aneuploidy (*4, 5*). Given that chromosome segregation errors occur mostly in female meiosis, particularly during the first meiotic division (Meiosis I, MI) (*6, 7*), it is crucial to understand the molecular mechanisms regulating female MI and how it can go wrong.

Oogenesis is a complex process that begins during fetal development in female mammalian species, shortly after conception. During late pregnancy, oocytes enter MI and duplicate their genome DNA (*8*). Shortly after birth, all germ cells undergo a prolonged arrest at the prophase I stage, which lasts until puberty. In adult ovaries, hormonal cues prior to ovulation stimulate the oocyte to resume meiosis (*8*). The nucleus (germinal vesicle, GV) typically localizes at the oocyte center in fully grown prophase I-arrested oocytes (*9*). Even if the nucleus is off-centered, these cortical nuclei can migrate towards the oocyte center by F-actin-mediated pressure gradient (*10-13*). A recent study suggested that oocytes lacking F-actin with off-centered nucleus positioning have altered transcriptional dynamics (*13*). However, the significance of central nucleus positioning remains largely unknown.

Upon meiotic resumption, prophase I-arrested oocytes undergo nuclear envelope breakdown (NEBD). During NEBD, the microtubule organizing centers (MTOCs) undergo a three-step fragmentation process before their clustering and sorting into two dominant spindle poles (*14-*

57 *17*). Since the spindle position dictates the cell division plane (*18*), the spindle must migrate to
58 the oocyte cortex to ensure the highly asymmetric meiotic division (*18-22*). Extruding a small
59 polar body (PB) through a highly asymmetric division is critical as it allows the egg to retain the
60 majority of the cytoplasmic storage of maternal RNAs and proteins, which are essential for the
61 early embryonic development (*23, 24*). However, it is still mysterious why the spindle initially
62 forms at the oocyte center, especially since it can increase the risk of symmetric division, leading
63 to infertility.
64
65 Here we show that the premature peripheral spindle positioning causes abnormal kinetochore-
66 microtubule (K-MT) attachments, chromosome misalignment and aneuploidy. Importantly, we
67 find that the initial central spindle positioning is critical to avoid the premature exposure to
68 cortical CDC42 signaling, which affects the fidelity of K-MT attachments through microtubule
69 tyrosination. Interestingly, we find that nucleus positioning, a major contributor for spindle
70 location, is a dynamic process that depends on maternal age. The majority of oocytes collected
71 from sexually mature mice had a centrally positioned nucleus, whereas prepubertal and
72 peripubertal mice had more oocytes with a peripherally positioned nucleus, potentially increasing
73 the risk of aneuploidy.
74

75 **RESULTS**

76 ***Peripheral GV oocytes have higher rates of misaligning chromosomes and forming aneuploid***
77 ***eggs***

78 In mouse oocytes, the meiotic spindle can initially form at the oocyte center (Supplementary Fig.
79 1A) or near the cortex (Supplementary Fig. 1B) depending on where NEBD occurs. To

80 investigate the impact of the initial spindle position on female meiosis, we sorted fully grown
81 prophase I-arrested oocytes into three groups based on the shortest distance between the nucleus
82 and the cortex: central (larger than 15 μm), intermediate (5 – 15 μm), and peripheral (less than 5
83 μm) GV oocytes (Fig. 1A,B). Careful rolling of the oocyte, as previously described (*9*), ensured
84 the correct classification. All oocytes selected for the following experiments were comparable in
85 size with a diameter larger than 80 μm (Supplementary Fig. 1C,D), indicating the full-grown
86 status (*25-27*). Any oocyte with a diameter less than 80 μm was removed from further
87 experiments to exclude the possibility of oocyte growth-associated nucleus centration (*9*). DNA
88 staining revealed that all selected oocytes, including peripheral GV oocytes, had a surrounded
89 nucleolus (Supplementary Fig. 1E), a criterion positively associated with developmental
90 competence (*28*). Finally, central GV oocytes were more common in 6-week-old mice compared
91 to intermediate GV oocytes and peripheral GV oocytes (Supplementary Fig. 1F).
92
93 Using the sorted oocytes, we examined the impact of the nucleus position on female meiosis. To
94 examine meiotic progression, oocytes were collected from mice aged 6-8 weeks and matured for
95 16 h (metaphase II). The majority (~92%) of central GV oocytes were able to undergo NEBD. In
96 contrast, peripheral GV oocytes showed a significant decrease in NEBD rate (~61%, Fig. 1C).
97 However, using time-lapse microscopy, we found no significant difference in the timing of
98 NEBD between central GV oocytes and peripheral GV oocytes (Fig. 1D). Similarly, a majority
99 (~81%) of central GV oocytes were able to extrude the first polar body (PBE), while peripheral
100 GV oocytes were less successful in extruding the first PB (~60%, Fig. 1E). Once again, there
101 was no significant difference in the timing of PBE between central GV oocytes and peripheral
102 GV oocytes (Fig. 1F). To examine the chromosome alignment and spindle morphology among

103 groups, oocytes were matured *in vitro* for either 7 h (metaphase I) or 16 h (metaphase II).
104 Chromosome alignment was examined based on to parameters previously described (*29*). We
105 found a significant increase in chromosome misalignment at both metaphase I and metaphase II
106 in peripheral GV oocytes, compared to central GV oocytes. Intermediate GV oocytes also
107 showed significantly higher rates of chromosome misalignment when compared to central GV
108 oocytes at metaphase I, but not at metaphase II (Fig. 1G,H and Supplementary Fig. 2A,B).
109 Spindle morphology did not vary significantly among groups either at metaphase I or metaphase
110 II (Fig. 1G,I and Supplementary Fig. 2A,C). Because chromosome misalignment is highly
111 associated with aneuploidy, we then assessed aneuploidy in metaphase II eggs using *in situ*
112 chromosome counting (*30, 31*). Strikingly, segregation errors occurred in peripheral GV oocytes
113 (~50.15%) approximately five times more frequently than in central GV oocytes (<8 %, Fig.
114 1J,K). Although we cannot exclude the effect of additional manipulating time (~ 30 minutes for
115 oocyte sorting/measurements) on oocyte quality, <8% aneuploidy in central GV oocytes remains
116 within the range of aneuploidy in control groups in several previous publications (*32, 33*).
117
118 ***Incorrect kinetochore-microtubule attachments are increased in oocytes with a peripherally***
119 ***located nucleus***
120 One important cause of aneuploidy is the weakened spindle assembly checkpoint (SAC).
121 Typically, the SAC monitors the status of K-MT attachments and will become inactivated when
122 MTs are correctly attached to all kinetochores. However, a weakened SAC may allow the
123 progression of the cell to anaphase without proper K-MT attachments, leading to aneuploidy. To
124 assess the SAC function in central, intermediate, and peripheral GV oocytes, oocytes were
125 treated with nocodazole, a MT depolymerizing drug that maintains the SAC active and thereby

126 prevents PBE by inducing metaphase I arrest (*31, 34*). We find that central, intermediate, and
127 peripheral GV oocytes all failed to extrude the PB in the presence of nocodazole. In contrast,
128 positive control oocytes treated with ZM447439, an Aurora Kinase B/C inhibitor that is known
129 to disrupt the SAC function at a high dose (10μM), extruded the PB even in the presence of
130 nocodazole (*35*) (Supplementary Fig. 2D). These results suggest that the SAC is intact in
131 peripheral GV oocytes, and therefore, not explaining their observed high aneuploidy rate.
132
133 Following spindle migration to the cortex, centromeres facing the cortex have less stable K-MT
134 attachments (*36*). These observations suggest that the cortex can influence MT dynamics and
135 their ability to establish stable attachments with kinetochores (*36*), a critical step to ensure
136 faithful chromosome segregation. In oocytes, even if the SAC is satisfied by present K-MT
137 attachments, it is not necessary that all attachments are correct and homologous chromosomes
138 are bioriented (*29, 37*). To assess K-MT attachments, metaphase I oocytes (~7 h) were exposed
139 to a brief cold shock (6 minutes) to depolymerize labile non-K-MTs and preferentially maintain
140 stable MT fibers that are attached to kinetochores (*31, 38*). Nucleus positioning had no effect on
141 the percentage of unattached kinetochores (Fig. 2A, Supplementary Fig. 2E). However,
142 peripheral GV oocytes displayed ~ four-fold increase in the percentage of incorrect K-MT
143 attachments, compared to central GV oocytes (Fig. 2A,B). Moreover, the percentages of
144 peripheral (37.93 ± 9.17%) and intermediate (39.13 ± 10.41%) GV oocytes having two or more
145 abnormally attached kinetochores were significantly higher than those in central GV oocytes
146 (7.14 ± 4.02%, Fig. 2C). These results suggest that improper K-MT attachments are the likely
147 cause, at least in part, of the increased aneuploidy rate in peripheral GV oocytes.
148

149 ***Prophase I oocytes favor central nucleus positioning***

150 When meiotic resumption was prevented (by milrinone treatment) in peripheral GV oocytes, the
151 nucleus relocated to the oocyte center within 3 h of incubation in the majority of oocytes
152 (Supplementary Fig. 3A,B and Movie 1), confirming that the nucleus favors the central position,
153 as previously reported (*10, 39, 40*). Central positioning of the nucleus is actin dependent.
154 However, there were no differences observed between oocytes with a centrally or a peripherally
155 located nucleus in terms of cytoplasmic F-actin, cortical F-actin, or perinuclear F-actin
156 (Supplementary Fig. 3C-F). When the oocytes were allowed to resume meiosis, in milrinone-free
157 medium, nuclei initially located at the periphery of the oocyte underwent significant central
158 movement (10 ± 1.256 μm) before undergoing NEBD. Intermediately located nucleus and
159 centrally located nucleus underwent central movement and traveled a distance of 6 ± 0.6024 μm
160 and 4 ± 0.6783 μm, respectively, before NEBD (Supplementary Fig. 4A). However,
161 chromosome alignment in oocytes with a peripherally located nucleus occured relatively closer
162 to the oocyte cortex in comparison to chromosome alignment in oocytes with a central nucleus
163 (Supplementary Fig. 4B,C). It is of note that the timing of chromosome alignment did not vary
164 significantly among groups (Supplementary Fig. 4D), suggesting that peripheral GV oocytes do
165 not exhibit a cell cycle delay. These results suggest that mouse oocytes favor central nucleus
166 positioning, likely to avoid the increased incidence of aneuploidy in peripheral GV oocytes.
167

168 ***Incidence of aneuploidy directly associates with the proximity of early spindle positioning to***
169 ***the cortex***

170 Because the spindle forms where NEBD occurs, whether at the center (Supplementary Fig. 1A)
171 or at the cortex (Supplementary Fig. 1B), it is likely that increased aneuploidy in peripheral GV

172 oocytes is, at least in part, due to peripheral spindle formation. Using live time-lapse microscopy,
173 we found that oocytes with a peripherally located nucleus demonstrate one of three types of
174 movement: oocytes that were able to achieve complete relocation of the nucleus to the center
175 prior to NEBD (the spindle is formed centrally) were termed 'corrected', oocytes that
176 demonstrated central movement prior to NEBD but did not achieve full relocation were termed
177 'migratory', and oocytes that failed to make a relocation attempt before NEBD and remained at
178 the cortex were termed 'peripheral' (the spindle is formed peripherally; Fig. 2D). Strikingly,
179 although all oocytes selected in this experiment were peripheral GV oocytes, oocytes that were
180 able to successfully relocate their nucleus to the center and experienced central spindle formation
181 showed relatively lower rates of aneuploidy when compared to oocytes that failed nucleus
182 relocation and underwent NEBD at the periphery of the oocyte (Fig. 2E,F). These results suggest
183 that peripheral GV oocytes are not inherently erroneous, but instead peripheral spindle formation
184 is detrimental to the fidelity of chromosome segregation.
185 After meiotic resumption, mouse oocyte spindles are typically formed and remained at the
186 oocyte center until late metaphase I (~7h) followed by their timely migration towards the cortex.
187 It is technically feasible to shift the position of the spindle within the oocyte without noticeable
188 adverse effects (*22, 41*). To further confirm the relationship between the aneuploidy rate and the
189 proximity of early spindle positioning to the cortex, we experimentally relocated the spindle
190 prematurely to the cortex through mild centrifugation (Fig. 2G), a technique proven successful in
191 murine oocytes (*42*). This centrifugation technique has been used extensively for several
192 purposes (*e.g.,* lipid droplet removal and prior to parthenogenetic activation) without noticeable
193 detrimental effects on oocyte developmental competence (*43-45*). Central GV oocytes were
194 selected and matured *in vitro* for 4 h, until prometaphase I (the time prior to establishing correct

195 K-MT attachments) (*46*). These prometaphase I oocytes were centrifuged, examined live under
196 the microscope and resorted into two groups according to their spindle positioning: those
197 maintaining central positioning (control central) and those with induced peripheral positioning
198 (induced peripheral), which was followed by *in vitro* maturation for an additional 13 h to reach
199 metaphase II. Importantly, although all oocytes were originally central GV oocytes, oocytes with
200 induced peripheral positioning showed significantly higher rates of aneuploidy when compared
201 to oocytes maintaining central spindle positioning after centrifugation (Fig. 2H,I), indicating that
202 the premature cortical proximity of the spindle (prior to establishing correct K-MT attachments)
203 causes erroneous chromosome segregation.
204
205 ***Premature exposure to the cortical CDC42 signal perturbs K-MT attachments in oocytes***
206 A conserved Rho-family GTPase, CDC42, is the master regulator of cell polarity in multiple
207 systems. To investigate whether the premature exposure of the spindle to the cortical cues
208 perturbs the establishment of correct K-MT attachments, we inhibited the cortical CDC42
209 signaling in prometaphase I oocytes with a peripherally located spindle. Peripheral GV oocytes
210 were matured *in vitro* for 5 h, and oocytes with a peripherally positioned spindle (confirmed
211 using Z-series live imaging) were selected and treated with ML141 (a previously proven
212 selective CDC42 inhibitor in mammalian oocytes) (*47-49*) for an additional 2 h (Fig. 3A).
213 Examining K-MT attachments in metaphase I oocytes showed that the number of unattached
214 kinetochores did not differ significantly among groups (Supplementary Fig. 5A). Inhibition of
215 CDC42 by using ML141 has no significant effect on cytoplasmic or cortical F-actin in oocytes
216 with a peripherally located spindle (Supplementary Fig. 6A-C) nor on K-MT attachments in
217 oocytes with a centrally located spindle (Fig. 3B,C). Importantly, inhibition of cortical CDC42

218 signals using ML141 partially rescued abnormal K-MT attachments in oocytes with a
219 peripherally positioned spindle (Fig. 3B,C). To further confirm this finding, we perturbed the
220 CDC42 signaling by overexpressing CDC42 dominant-negative mutant (CDC42 T17N,
221 previously demonstrated to inhibit CDC42 in mouse oocytes) (*50*). Consistent with the ML141
222 results, perturbing CDC42 signaling by overexpressing a CDC42 dominant-negative mutant
223 significantly rescued abnormal K-MT attachments in oocytes with a peripherally located spindle
224 (Fig. 3D,E). Taken together, these results suggest that the increased incidence of abnormal K-
225 MT attachments in oocytes with a peripherally located spindle is, at least in part, due to the
226 premature exposure to cortical CDC42 signaling.
227 Induced peripheral oocytes (*i.e.* oocytes with a peripherally located spindle after centrifugation)
228 exhibited higher rates of abnormal K-MT attachments, compared to those that maintained a
229 centrally positioned spindle (control central) after centrifugation (Supplementary Fig. 5B,D). To
230 confirm that K-MT attachments in induced peripheral oocytes were affected primarily by the
231 proximity to the cortex and to exclude the possibility that the difference in the response to
232 centrifugation between induced peripheral and control central oocytes was due to a pre-existing
233 difference, we asked whether inhibiting CDC42 cortical signals could rescue the increased
234 incidence of abnormal K-MT attachments in induced peripheral oocytes. Control central and
235 induced peripheral prometaphase I (5 h) oocytes were treated with or without ML141 for an
236 additional 2 h prior to assessing K-MT attachments (Supplementary Fig. 5B). There were no
237 differences in the percentage of unattached kinetochores among groups (Supplementary Fig. 5C).
238 Importantly, CDC42 inhibition largely rescued the increased incidence of abnormal K-MT
239 attachments in induced peripheral oocytes (Supplementary Fig. 5D), further supporting the idea
240 that increased abnormal K-MT attachments in induced peripheral oocytes is due to the premature

241 exposure of the spindle to the cortical CDC42 signal. Collectively, these results strongly suggest
242 that avoiding the cortical CDC42 signal during prometaphase I (*i.e.* by being at the oocyte center
243 prior to timely spindle migration) is critical in protecting the oocyte's ability to establish correct
244 K-MT attachments, leading to faithful chromosome segregation.
245
246 ***Excessive MT tyrosination interferes with establishing correct K-MT attachments***
247 We next asked how CDC42 affects K-MT attachments. Because the cortical CDC42 plays an
248 essential role in actin cap formation by activating ARP2/3 complex (*51*), we tested whether
249 CDC42 signaling perturbs K-MT attachments in peripheral GV oocytes via the premature
250 activation of ARP2/3. To address this question, peripherally GV oocytes were matured *in vitro*
251 for 5 h and oocytes with a peripherally positioned spindle (confirmed using Z-series live
252 imaging) were treated with CK-666 (a selective and potent ARP2/3 inhibitor) (*51, 52*) for an
253 additional 2 h. Analyzing K-MT attachments in metaphase I oocytes showed that ARP2/3
254 inhibition did not rescue abnormal K-MT attachments in oocytes with a peripherally located
255 spindle (Supplementary Fig. 6D,E), indicating that CDC42 signaling does not perturb the
256 establishment of K-MT attachments via actin cap formation.
257 Recent study using mouse oocytes suggested that CDC42 signaling can promote α-tubulin
258 tyrosination within the cortical spindle, increasing MT dynamics (*36*). Therefore, we
259 hypothesized that the premature exposure of the spindle to cortical CDC42 (*i.e.* before
260 establishing correct K-MT attachments) results in excessive MT tyrosination, which interferes
261 with the correction mechanism of K-MT attachments. The genetically encoded C-terminal
262 tyrosine on α-tubulin undergoes cycles of detyrosination and (re) tyrosination (*53*). In mitotic
263 cells, initial incorrect attachments are established during early mitosis and primarily formed by

264 tyrosinated MTs. Tyrosinated MTs are relatively labile to depolymerization, leading to their
265 detachment from chromosomes. When correct attachments are established, MTs are
266 detyrosinated and stabilized (*54*). In mouse oocytes, reducing α-tubulin tyrosination (by
267 depleting tubulin-tyrosine ligase) increased the rate of MT stabilization (*36*). Thus, the level of
268 MT tyrosination must be spatiotemporally regulated to establish correct K-MT attachments. To
269 test whether α-tubulin tyrosination levels depend on the spindle position, we compared
270 tyrosinated α-tubulin levels in metaphase I oocytes between central and peripheral spindles. In
271 contrast to β-tubulin levels, which were not affected by the spindle position, tyrosinated α-
272 tubulin levels were significantly higher in oocytes with a peripherally positioned spindle when
273 compared to oocytes with a centrally positioned spindle (Fig. 4A,B). We also confirmed the
274 impact of CDC42 signaling on α-tubulin tyrosination in the spindle. Our results showed that
275 tyrosinated α-tubulin levels were significantly lower in CDC42-inhibited oocytes (oocytes
276 expressing CDC42 dominant negative mutant, CDC42 T17N), compared to control oocytes (Fig.
277 4C,D). Thus, CDC42 cortical signaling promotes MT tyrosination in mouse oocytes. We then
278 asked whether decreasing tyrosination levels could rescue increased abnormal K-MT
279 attachments in peripheral GV oocytes. Removing the tyrosine residue from α-tubulin (*i.e.*
280 detyrosination) is regulated by tubulin carboxypeptidase enzymes encoded by Vasohibins
281 (VASHs) (*55, 56*). Ectopic expression of VASH2 did not completely abolish tyrosinated α-
282 tubulin in mouse oocytes (Fig. 4E), whereas co-expression of VASH2 and small VASH binding
283 protein (SVBP, a chaperone protein required for VASH stability) (*55, 56*) eliminated tyrosinated
284 α-tubulin without affecting the bipolar spindle formation (Fig. 4E-G, Supplementary Fig. 7).
285 Importantly, decreasing α-tubulin tyrosination significantly decreased abnormal K-MT
286 attachments in oocytes with a peripherally located spindle (Fig. 4H,I). Taken together, our data

287 indicate that the premature exposure of the spindle to cortical CDC42 signaling interferes with
288 the establishment of correct stable K-MT attachments, via promoting MT tyrosination.
289

290 ***Too young female mice tend to have peripheral GV oocytes increasing the risk of aneuploidy***

291 It is established that the egg aneuploidy rate increases with advanced maternal age mainly due to
292 chromosome cohesion loss. However, it is becoming increasingly clear that too young females
293 also have higher chances of producing aneuploidy eggs(*5*), though the underlying mechanisms
294 are largely unknown. We wondered if the nucleus position may explain the higher aneuploidy
295 rate in younger females. To test this idea, we quantified the nucleus position *in vivo* by analyzing
296 ovary sections from mice with different ages (2-, 3-, 5-, and 8-week-old) (Fig. 5A-C). We found
297 that the majority of oocytes were categorized as central GV oocytes for the 8-week-old mice, but
298 the younger mice (2-, 3-, and 5-week-old) had fewer central GV oocytes, and the peripheral GV
299 oocytes were the majority in the 2- and 3-week-old mice (Fig. 5A-C). *In vitro*-cultured oocytes
300 from 2-, 3-, 5-, and 8-week-old mice showed similar trends with the *in vivo* experiment (Fig.
301 5D). These results suggest that oocytes from very young mice tend to have a peripheral nucleus,
302 possibly increasing their aneuploidy risk through the premature exposure of the spindle to
303 cortical cues.
304

305 **DISCUSSION**

306 Aneuploidy occurs frequently in female oocytes, typically as a result of mis-segregation during
307 MI (*6, 7, 33, 57*). We developed different complementary and confirmatory oocyte models in
308 which: 1) the spindle is assembled peripherally or centrally (based on the nucleus position or the
309 location of the spindle at NEBD), 2) the centrally positioned spindle is prematurely relocated

310 towards the cortex (using centrifugation), or 3) cortical CDC42 signaling is perturbed in oocytes
311 with a peripherally located spindle. We found that initial spindle positioning at the oocyte center
312 (until proper K-MT attachments are established and prior to timely spindle migration) is an
313 insurance mechanism to avoid the premature exposure to cortical CDC42 signaling, which
314 hinders proper K-MT attachments, leading to aneuploidy. These findings may explain why, in
315 mouse oocytes, correct K-MT attachments are primarily established when the spindle is still at
316 the oocyte center (~ 2 h before anaphase I), *i.e.* before migrating to the cortex (*36, 46*).
317
318 Nucleus positioning in meiotic oocytes is often studied only *in vitro* or at a single time point *in*
319 *vivo* and, thus, the comprehensive understanding across different timepoints is missing. Also,
320 there has been a long-standing debate regarding the position of the nucleus in mouse oocytes. For
321 example, a previous study found that the majority of prophase I-arrested oocytes have a
322 peripherally located nucleus, and this cortical positioning of the nucleus is likely influenced by
323 gap junctions and increased cumulus cell contact (*58*). On the other hand, other studies
324 demonstrated that the majority of prophase I-arrested oocytes have a centrally positioned nucleus
325 (*9, 13, 59*). Interestingly, in the first study (*58*), the oocytes were collected from mice aged 21
326 days, whereas in the other studies (*9, 13, 59*), the oocytes were collected from mice aged more
327 than 6-8-weeks old. Our results clearly link these previous findings, providing an explanation to
328 the long-standing debate on the nucleus position in mouse oocytes and advancing our
329 understanding of an important phenomenon.
330
331 Although the nucleus shifts from a peripheral position in prepubertal oocytes towards a central
332 position in sexually mature mouse oocytes, this is likely not the only shift during the

333 reproductive life. Indeed, it has been shown that oocytes from aged mice (~1 year) also exhibit a
334 majority of peripherally positioned nuclei (*9*). These observations indicate that oocyte nucleus
335 migrates to the oocyte center during sexual maturation and migrates back to the cortex with the
336 advancement of maternal age. Investigating the molecular basis underlying the age-dependent
337 nucleus migration would be an interesting future direction. For example, analyzing cytoskeleton
338 dynamics at different developmental stages may reveal why the nucleus migrates towards certain
339 directions at certain stages.
340
341 Nucleus relocation within eukaryotic cells is critical for organism development. In *Drosophila*
342 oocytes, the nucleus migrates from a central posterior to an asymmetrical anterior position to
343 dictate the dorsal-ventral axis, necessary for organogenesis and *Drosophila* development (*60-62*).
344 In *C. elegans* zygotes, the two pronuclei meet at the posterior cortex and then migrate towards
345 the zygote center to allow proper spindle pole orientation along the anterior-posterior axis prior
346 to spindle migration towards the posterior cortex (*63-66*). Although many mammalian oocytes at
347 prophase I are not polarized and the nucleus position has no consequence on the developmental
348 axis, they still employ a similar nucleus relocation. The peripheral nucleus undergoes centration
349 which correlates with maturation success. Following NEBD, the centrally formed spindle must
350 migrate towards the cortex in a timely manner to ensure the asymmetric division. Our
351 understanding of the biological significance of central nucleus positioning in mammalian oocytes
352 is still rudimentary. It has been proposed in Almonacid *et al*. (2018) that nucleus centration plays
353 a role in keeping prophase I oocytes in a non-polarized state, ensuring random cytoplasmic
354 distribution and avoiding unphysiological cytoplasmic compartmentalization (*11*). Our findings
355 suggest that central nucleus positioning is an insurance mechanism to allow the avoidance of the

356 spindle to the premature exposure to cortical cues, providing a complementary explanation of
357 why mouse oocytes experience nucleus centration.
358
359 Current *in vitro* fertilization (IVF) technologies have much room for improvement, as only
360 12.7% of naturally ovulated IVF cycles in humans lead to pregnancy and only 8.8% of those
361 pregnancies result in live births (*67*). Although technologies and protocols have advanced since
362 the first IVF birth in 1978, the IVF success rate remains less than 50% for women under the age
363 of 35 (*68*). To date, there are no definitive morphological markers of predictive oocyte
364 aneuploidy. Gametes from human females are notoriously associated with high rates of
365 aneuploidy (*4, 6*). In addition, human oocytes with a peripherally located nucleus are associated
366 with poor maturation rates compared to those with a centrally located nucleus (*59*). Therefore, it
367 is tempting to speculate that central nucleus positioning is a strategy to ensure initial spindle
368 positioning at the oocyte center, thereby avoiding the development of aneuploid gametes.
369 Understanding the association between peripherally located spindle and the incidence of
370 aneuploidy may allow us to better screen for the oocytes predisposed to proper chromosome
371 segregation.
372

373 **MATERIAL AND METHODS**

374 ***Ethics***

375 All laboratory animals were managed, and experiments conducted, in compliance with the
376 University of Missouri (Animal Care Quality Assurance Reference Number, 9695).
377

378 ***Mouse strains***

379 Unless otherwise specified, female CF-1 WT mice were used. *Cep192-eGfp* reporter mice were
380 generated (*69*) by integrating a construct harboring the EGFP reporter gene into CF-1 mouse
381 genome via CRISPR/Cas9-mediated homology-directed repair. The EGFP reporter was fused at
382 the C-terminus of the endogenous mouse Cep192. Homozygous breeding pairs of *Cep192-eGfp*
383 reporter mice were used to maintain the colony.
384
385 ***Oocyte collection, microinjection and in vitro maturation (IVM)***
386 Full-grown GV oocytes were collected from CF-1 female mice aged 6-8 weeks. Oocyte
387 collection and culture were carried out as previously described (*31, 70*). Cumulus oocyte
388 complexes (COCs) were collected and cultured in bicarbonate-free minimal essential medium
389 (MEM) supplemented with 3mg/ml polyvinylpyrrolidone (PVP) and 25 mM HEPES (pH 7.3)
390 under mineral oil (MilliporeSigma, St. Louis, MO, USA # P2307, # H3784, # M8410). Oocytes
391 were manually denuded and sorted into 3 groups: Central GV, Intermediate GV, Peripheral GV
392 oocytes. Careful rolling of the oocyte, as previously described, ensured correct classification (*9*).
393 Denuded GV oocytes were microinjected with ~5 pl of the indicated cRNA using Eppendorf
394 Femtojet 4i. The injection medium for oocytes was MEM supplemented with 3mg/ml
395 polyvinylpyrrolidone (PVP), 25 mM HEPES (pH 7.3) under mineral oil. Oocytes were then
396 transferred to Chatot, Ziomek, and Bavister (CZB) maturation medium (*71*) supplemented with
397 1μM glutamine (MilliporeSigma, # G8549) under mineral oil and matured at 37˚C with
398 humidified 5% CO_2 in an incubator for either 7, 14, or 16 h.
399 Nocodazole (Sigma #M1404), monastrol (Sigma #M8515), ML141 (Sigma #SML0407),
400 ZM447439 (Tocris #2458) and CK-666 (Sigma #182515) were dissolved in DMSO and added to
401 CZB culture medium at a final concentration of 5 μm, 100 μM, 500 nM, 10 μm and 50 μM,

402 respectively. SiR-tubulin and SiR-DNA were added to the maturation medium (at a final
403 concentration of 100 nM) during live imaging to label MTs and DNA, respectively.
404

405 ***In vitro cRNA synthesis***

406 Synthesis of cRNAs was performed using T7 polymerase (mMessage mMachine kit, Ambion)
407 according to the manufacturer's instructions. The cRNA was purified using an RNAEasy kit
408 (Qiagen). cRNAs used for microinjection were 3xFLAG-Vash2 (mouse VASH2 with three
409 tandem FLAG tag at the N terminus) at 500 ng/µl, SVBP-HA (mouse SVBP with a HA tag at the
410 C terminus) at 300 ng/µl and *Cdc42 T17N* (dominant-negative CDC42 mutant) at 800 ng/µl.
411

412 ***Immunocytochemistry***

413 After maturation, oocytes were fixed in a freshly prepared solution of 3.7% paraformaldehyde
414 (MilliporeSigma, # P6148) dissolved in phosphate buffer saline (PBS). Oocytes were incubated
415 in permeabilization solution (0.1% Triton X-100 in PBS) for 20 minutes and blocking solution
416 (0.3% BSA and 0.01% Tween-20 in PBS) for 20 minutes before staining. Oocytes were
417 incubated at room temperature for one h with the primary antibody before undergoing 3
418 consecutive washes in blocking solution for 9 minutes each. Oocytes were then incubated at
419 room temperature for one h in the secondary antibody solution. Phalloidin (ThermoFisher
420 Scientific #T7471; 1:50) was added to the secondary antibody solution to label F-actin.
421 Following another 3 consecutive washes in blocking solution at 9 minutes each, oocytes were
422 mounted on glass slides using Vectashield containing 4',6-Diamidino-2-Phenylindole,
423 Dihydrochloride (DAPI; Vector Laboratories, Burlingame, CA, USA) in order to stain the DNA.
424 Fluorescence was observed using a 40X oil objective using Leica TCS SP8 confocal microscope

425 or Leica DMI8 fluorescence microscope and oocytes were imaged using 3 µm Z-intervals.
426 Oocytes were analyzed using NIH ImageJ software (National Institute of Health, Bethesda, MD
427 USA).
428 The following primary antibodies were used in immunofluorescence: conjugated α-tubulin-
429 AlexaFluor 488 (Life Technologies # 322 588; 1:75), CREST autoimmune serum (Antibodies
430 Incorporated # 15-234; 1:25), tyrosinated α-tubulin (BIO-RAD# MCA77G; 1:500), and anti β-
431 tubulin (9F3) monoclonal conjugated to Alexa Fluor 488 (Cell Signaling Technology, #3623;
432 1:50).
433
434 ***In situ chromosome counting***
435 Oocytes matured *in vitro* for 14 h in CZB medium supplemented with L-glutamine under mineral
436 oil were transferred to CZB containing 100 µm monastrol (MilliporeSigma, # M8515) and
437 incubated an extra 2 h; monastrol is an Eg5-kinesin inhibitor which induces monopolar spindle
438 formation and thus results in a rosette of chromosome distribution (*30, 31*). After treatment with
439 monastrol, oocytes at metaphase II stage were fixed in a freshly prepared solution of 2.5%
440 paraformaldehyde (MilliporeSigma, # P6148) and stained with CREST autoimmune serum
441 (Antibodies Incorporated # 15-234; 1:25) to label the kinetochores. DAPI was used to label the
442 DNA. Fluorescence was observed using a 40X oil objective using a Leica DMI8 microscope and
443 oocytes were imaged using 0.5 µm Z-intervals in order to observe all kinetochores. Oocytes were
444 analyzed individually and were scored either as euploid (containing 40 kinetochores) or as
445 aneuploid (containing ± 40 kinetochores).
446
447 ***Assessment of kinetochore-microtubule attachment***

448 Cells were matured *in vitro* for 7 h in CZB medium supplemented with L-glutamine under
449 mineral oil. The oocytes were placed on ice for 6 minutes in a 96 well dish containing chilled
450 MEM. Exposing the oocytes to cold shock depolymerizes unattached MTs; however, when MTs
451 have established end-on attachment to a kinetochore, it becomes cold stable (*38*). Oocytes were
452 fixed using a freshly prepared 2.5% paraformaldehyde solution and immunostained with anti-
453 human CREST (to label kinetochores) and α-tubulin (to label MTs) antibodies. DAPI was used
454 to label DNA. Cells were imaged using a Leica TCS SP8 confocal microscope and a x63 oil
455 objective, taking images at 0.5 µm Z-intervals. Kinetochores were scored as normal (attached to
456 bioriented chromosomes), unattached, or abnormally attached (syntelic - kinetochores of both
457 homologous chromosomes attached to one side of the spindle or merotelic - a kinetochore
458 maintaining attachment to both sides of the spindle), as previously described (*31*). Oocytes were
459 analyzed using NIH ImageJ Software.
460
461 ***Time-lapse microscopy***
462 Full-grown oocytes were imaged using a 40X oil objective on Leica TCS SP8 confocal
463 microscope or Leica DMI8 microscope within a microenvironmental chamber maintaining an
464 atmosphere of 5% CO_2 and temperature of 37˚C in humidified air. Imaging acquisition began
465 before NEBD. Images were captured at 5 µm Z-intervals. Image sequences were analyzed using
466 NIH ImageJ Software.
467
468 ***Ovary collection and histological evaluation***
469 Ovaries from CF-1 mice of varying ages (2 weeks, 3 weeks, 5 weeks, and 8 weeks) were
470 collected, submerged, and stored in buffered zinc formalin overnight. Tissues were then moved

471 to 70% ethanol for storage until undergoing a 10-h protocol using a Leica ASP300S enclosed
472 tissue processor. After processing, tissues were embedded in paraffin wax and cooled fully using
473 the Leica EG1150 C/H pair. Embedded tissues were sectioned at 8 µm thickness using a Leica
474 Histocore AutoCut microtome. Representative samples were taken for each age by taking 3
475 consecutive sections periodically (every 4, 6, 8, or 10 sections respectively). Tissues were
476 stained with Hematoxylin and Eosin (Abcam, # 245880) before being mounted with permount
477 resin (Thermo Fisher Scientific, Inc. # SP15). Oocytes and their corresponding nucleus
478 positioning were examined using 10X or 40X objective on a Leica DMI8 microscope.
479
480 ***Statistical analysis***
481 Tests used to evaluate the statistical significance of the findings reported include One-way
482 ANOVA and Student t-test using GraphPad Prism. The Tukey post hoc test was utilized to
483 determine statistical significance between groups. Student's t-test was performed for normally
484 distributed numerical data following D'Agnostino-Pearson omnibus normality test. P values of <
485 0.05 were considered significant. All data are displayed as means ± SEM.
486

487 Declaration of interest

488 All authors declare that there are no conflicts of interest that may prejudice or bias the research
489 reported.
490

491 Funding

492 This research was supported by laboratory start-up funding from the University of Missouri and
493 the NIH (R35 GM142537) to AZB and the Division of Intramural Research at the

National Institutes of Health/National Heart, Lung, and Blood Institute (1ZIAHL006249-01) to TA.

Acknowledgements

The authors would like to thank all members of the Balboula lab at the University of Missouri, Columbia for dedicated help and encouragement. The authors would like to thank Rocio Rivera, Heide Schatten for critical reading of the manuscript and valuable discussion, Yuksel Agca, Pramod Dhakal, Thomas Spencer, the Animal Modeling Core and the Molecular Cytology Core for valuable discussion and equipment usage, and Guillaume Halet for providing the CDC42 T17N construct.

Author Contributions

AZB conceived the project. AZB, JK and TA designed and analyzed experiments. JK, AH, TA and AZB performed experiments. AZB and JK wrote the manuscript. All authors read/edited the manuscript.

512 ## Figure Legends

513 **Figure 1: Oocytes with a peripherally located nucleus have higher rates of chromosome**
514 **misalignment and aneuploidy.**

515 (A) Full-grown GV oocytes were collected, imaged, and classified into one of three groups:
516 central GV, intermediate GV, or peripheral GV according to the distance measured from the
517 nucleus to the nearest cortex. The scale bar represents 50 μm. Oocyte diameter is included in the
518 top left of each image in white text; distance from the germinal vesicle to the cortex is included
519 above the scale bar in red text. (B) Quantification of the average distance from the nucleus to the
520 nearest cortex within groups (right graph). (C-F) Full-grown prophase I-arrested oocytes were
521 collected and sorted into central, intermediate and peripheral groups based on nucleus
522 positioning and imaged live using time-lapse microscopy during *in vitro* maturation. (C)
523 Quantification of the percentage of oocytes that underwent NEBD. (D) Quantification of the
524 average time of NEBD. (E) Quantification of the percentage of first polar body extrusion (1st
525 PBE). (F) Quantification of the average time of PBE calculated from oocytes successfully
526 extruded the PB. (G-I) Full-grown prophase I oocytes were collected and sorted into central,
527 intermediate and peripheral groups based on nucleus positioning and *in vitro* matured for 7 h
528 (metaphase I). Oocytes were fixed and immunostained with α-tubulin to label the microtubules
529 (the spindle). DNA was labeled by DAPI. (G) Representative confocal images of metaphase I
530 oocytes. (H) Quantification of the percentage of chromosome misalignment in metaphase I
531 oocytes. (I) Quantification of the percentage of abnormal spindle morphology in metaphase I
532 oocytes. Spindle morphology was assessed using the criterion that a normal meiotic spindle is
533 barrel shaped with two clearly defined spindle poles. (J) Full-grown prophase I oocytes were
534 collected and sorted into central, intermediate and peripheral groups based on nucleus

535 positioning and *in vitro* matured for 14 h (metaphase II). Oocytes were treated with monastrol for
536 2 h, fixed and immunostained with CREST antibody to label kinetochores. DNA was labeled by
537 DAPI. Oocytes were analyzed individually and scored either as euploid (containing 40
538 kinetochores) or as aneuploid (containing ± 40 kinetochores). Shown are representative images.
539 (K) Quantification of the percentage of aneuploid eggs. The scale bar represents 10 µm. One-
540 way ANOVA and Tukey's post hoc tests were performed to determine statistical significance
541 among groups. Data are displayed as mean ± SEM. Values with asterisks vary significantly, * P
542 <0.05, *** P <0.001, **** P <0.0001. The total number of analyzed oocytes (from at least 3
543 independent replicates) is specified above each graph.
544
545 **Figure 2: Incidence of incorrect K-MT attachments and aneuploidy associate with spindle**
546 **proximity to the cortex.**
547 (A) Representative images of kinetochore-microtubule (K-MT) attachments in oocytes with a
548 central, intermediate, or peripherally located nucleus matured to metaphase I and immunostained
549 with α-tubulin (to label MTs), CREST (to label kinetochores), stained with DAPI (to label
550 DNA), and imaged using confocal microscopy. Panels on the right (from top to bottom) display
551 normal K-MT attachment, unattached kinetochores and abnormal K-MT attachment. The scale
552 bar represents 10 µm. (B) Quantification of abnormal K-MT attachments. (C) Quantification of
553 the oocytes with 2 or more incorrect K-MT attachments. One-way ANOVA and Tukey's post
554 hoc test were performed to analyze the data. (D) Representative images of the nucleus movement
555 prior to NEBD. Images were taken every 30 minutes (Z-interval of 5 µm). The black circle
556 denotes the primary nucleus positioning, while the green circle denotes the final nucleus position
557 prior to NEBD. The scale bar represents 50 µm. (E) Representative images of aneuploidy in

558 oocytes experiencing full migration of the nucleus (corrected/central), attempted migration of
559 their nucleus (migratory), or not attempting central migration of the nucleus (peripheral). The
560 scale bar represents 10 µm. (F) Quantification of the incidence of aneuploidy in metaphase II
561 oocytes from the oocytes categorized in D. One-way ANOVA and Tukey's post hoc test were
562 performed to analyze the data. (G) Schematic depicting the induction of peripheral spindle
563 positioning by mild centrifugation in oocytes collected with a centrally positioned nucleus. (H)
564 Representative images of aneuploidy in oocytes either maintaining central spindle positioning
565 after centrifugation or induced peripheral spindle positioning after centrifugation. The scale bar
566 represents 10 µm. (I) Quantification of the incidence of aneuploidy in oocytes with induced
567 peripherally positioned nucleus and centrally positioned nucleus after centrifugation. Student t-
568 test was performed to determine statistical significance. Data are displayed as mean ± SEM.
569 Values with asterisks vary significantly, * $P < 0.05$, ** $P < 0.01$, **** $P < 0.0001$. The total
570 number of analyzed oocytes (from 3 independent replicates) is specified above each graph.
571
572 **Figure 3: Cortical CDC42 signaling impairs proper K-MT attachments in oocytes with**
573 **peripherally located spindles.**
574 (A) Schematic depicting the treatment of collected oocytes with ML141, a CDC42 inhibitor, in
575 order to inhibit the cortical influence upon kinetochore-microtubule (K-MT) attachment
576 formation. (B) Representative images of DMSO and ML141-treated oocytes matured to
577 metaphase I and immunostained with α-tubulin (to label MTs), CREST (to label kinetochores),
578 stained with DAPI (to label DNA), and imaged using confocal microscopy to assess K-MT
579 attachments. (C) Quantification of the average incidence of abnormal K-MT attachment in B.
580 (D) Representative images of K-MT attachment in oocytes expressing CDC42 dominant

581 negative mutant (CDC42 T17N). The scale bar represents 10 μm. (E) Quantification of the
582 average incidence of abnormal K-MT attachment in D. The scale bar represents 10 μm. One-way
583 ANOVA and Tukey's post hoc test were performed to determine statistical significance. Data are
584 displayed as mean ± SEM. Values with asterisks vary significantly, * P <0.05, ** P <0.01. The
585 total number of analyzed oocytes (from 3 independent replicates) is specified above each graph.
586
587 **Figure 4: Reducing tubulin tyrosination in peripheral GV oocytes rescued the abnormal K-**
588 **MT attachments.**
589 (A) Representative images of oocytes with centrally and peripherally located spindles stained for
590 tyrosinated α-tubulin and β-tubulin. (B) Quantification of tubulin intensities within the spindle.
591 (C) Representative images of oocytes expressing CDC42 dominant negative mutant (CDC42
592 T17N) stained for tyrosinated α-tubulin. (D) Quantification of tyrosinated α-tubulin levels
593 within the spindle. (E,F) Representative images of oocytes expressing VASH2 and
594 VASH2/SVBP stained for tyrosinated α-tubulin (E) and β-tubulin (F). (G) Quantification of
595 tubulin intensities within the spindle. (H) Representative images of K-MT attachment in
596 peripheral GV oocytes expressing VASH2 and VASH2/SVBP. (I) Quantification of abnormal K-
597 MT attachments in H. The scale bar represents 10 μm. One-way ANOVA and Tukey's post hoc
598 test were performed to determine statistical significance. Data are displayed as mean ± SEM.
599 Values with asterisks vary significantly, * P <0.05, ** P <0.01, *** P <0.001. The total number
600 of analyzed oocytes is specified above each graph.
601
602 **Figure 5: Nucleus positioning is a dynamic process throughout the development**

603 (A) Histological analysis of nucleus positioning *in vivo* at different ages. Ovaries from 2, 3, 5,
604 and 8 weeks old mice were collected, fixed, and stained with Hematoxylin and Eosin. Sections
605 were observed through 10X and 40X objective magnification and classified into one of the three
606 positioning groups: central, intermediate, peripheral. The scale bar represents 100 µm. (B)
607 Representative images of nucleus positioning in 3 and 8 weeks old mice. The white box
608 emphasizes the location of the magnified image within the ovary. The scale bar represents 100
609 µm. (C) Quantification of the *in vivo* proportion of oocytes sorted according to their nucleus
610 positioning (central, intermediate, peripheral) in 2, 3, 5, and 8 week old mice. (D) Quantification
611 of the in vitro proportion of oocytes sorted according to their nucleus positioning (central,
612 intermediate, peripheral) in 2, 3, 5, and 8 week old mice. Two-way ANOVA and Sidak's
613 multiple comparison test were performed to determine if the groups differed significantly. Data
614 are displayed as mean ± SEM. Values with asterisks vary significantly, * $P < 0.05$, ** $P < 0.01$,
615 *** $P < 0.001$, **** $P < 0.0001$. The total number of analyzed oocytes (from 3 independent
616 replicates) is specified above each graph.
617
618

619 **Supplementary Figures**

620 **Supplementary Figure 1:** Full-grown prophase I-arrested oocytes were collected from *Cep192-*
621 *eGfp* reporter mice, sorted into central (A) and peripheral (B) groups based on the positioning of
622 their nucleus and *in vitro* matured in CZB medium containing SiR-tubulin (to label microtubules,
623 magenta). Spindle poles were labeled by CEP192-EGFP (MT organizing centers, green).
624 Oocytes were imaged live using time-lapse confocal microscopy. Shown are representative
625 fluorescence and bright-field (lower panels) image sequence depicting the location of NEBD and
626 consequent spindle formation. Images were taken every 1 h (Z-projection of 13 sections every 5
627 μm). The scale bar represents 50 μm. (C) Oocytes were sorted based on location of their nucleus
628 into central or peripheral groups, imaged and quantified according to their diameter to ensure
629 similarity between groups. Please note that the large oocyte (105.97 μm, peripheral group) was
630 undergoing cell death and excluded from further experiments. (D) Quantification of the average
631 diameter of oocytes collected for experimentation. (E) Representative fluorescent image of
632 Hoechst staining (to label DNA) in group of selected, but not sorted, oocytes. Representative
633 images of oocytes with a peripherally located nucleus and a surrounded nucleolus are featured in
634 the right panel. The scale bar represents 50 μm. (F) Quantification of nucleus position in oocytes.
635 One-way ANOVA and Tukey's post hoc test were performed to analyze the data. Data are
636 displayed as mean ± SEM. Values with asterisks vary significantly, **** $P < 0.0001$. The total
637 number of analyzed oocytes is specified above each graph.

638

639 **Supplementary Figure 2:** Full-grown prophase I oocytes were collected and sorted into central,
640 intermediate and peripheral groups based on nucleus positioning and in vitro matured for 16 h
641 (metaphase II). Oocytes were fixed and immunostained with a-tubulin to label the microtubules

642 (the spindle). DNA was labeled by DAPI. (A) Representative confocal images of metaphase II
643 oocytes. (B) Quantification of the percentage of chromosome misalignment in metaphase II
644 oocytes. (C) Quantification of the percentage of abnormal spindle morphology in metaphase II
645 oocytes. Spindle morphology was assessed using the criterion that a normal meiotic spindle is
646 barrel shaped with two clearly defined spindle poles. The scale bar represents 10 µm. (D)
647 Quantification of successful polar body extrusion (1st) in oocytes treated with nocodazole.
648 ZM447439 oocytes served as a control. (E) Quantification of the percentage of unattached
649 kinetochores in central, intermediate, peripheral oocytes from Fig. 2A. One-way ANOVA and
650 Tukey's post hoc tests were performed to determine statistical significance among groups. Data
651 are displayed as mean ± SEM. Values with asterisks vary significantly, * $P < 0.05$, **** P
652 < 0.0001. The total number of analyzed oocytes (from at least 3 independent replicates) is
653 specified above each graph.
654
655 **Supplementary Figure 3:** (A) Representative bright-field images of time-lapse microscopy of
656 the movement of a peripherally positioned nucleus during prophase I arrest in oocytes incubated
657 with milrinone. Images were taken every 10 minutes using a Z-interval of 5 µm. The black circle
658 identifies the initial positioning of the nucleus, while the green circle denotes the final
659 positioning of the nucleus. The scale bar represents 50 µm. (B) Quantification of the percentage
660 of peripheral and intermediate GV oocytes achieving full relocation of the nucleus to a central
661 position within 3 h of incubation with milrinone. (C) Representative fluorescent image of F-actin
662 populations within oocytes. Enlarged panels featured to the right show, from top to bottom, areas
663 containing cytoplasmic, cortical, and perinuclear F-actin. The scale bar represents 50 µm. (D-F)
664 Quantification of the relative intensity of cytoplasmic, cortical, and perinuclear F-actin in

665 oocytes with either a centrally or peripherally positioned nucleus. Student t-test was performed to
666 determine statistical significance. Data are displayed as mean ± SEM.
667
668 **Supplementary Figure 4:** Full-grown prophase I-arrested oocytes were collected and sorted into
669 central, intermediate, and peripheral groups based on the positioning of their nucleus and imaged
670 live using time-lapse microscopy during *in vitro* maturation. (A) Quantification of the change in
671 the distance of the nucleus to the nearest cortex from the initial position of the nucleus at the
672 prophase I-arrested stage to the final destination of the nucleus immediately prior to NEBD. (B)
673 Representative fluorescence and bright-filed image sequence depicting chromosome alignment
674 (labeled by SiR-DNA, red) in oocytes with a peripheral (upper) and central (lower) nucleus.
675 Images were taken every 45 minutes using a Z-interval of 7 µm. Scale bars represent 50 µm. (C)
676 Quantification of the distance of chromosomes at the time of alignment to the nearest cortex. (D)
677 Quantification of the time of chromosome alignment. One-way ANOVA and Tukey's post hoc
678 test were performed to determine statistical significance. Data are displayed as mean ± SEM.
679 Values with asterisks vary significantly, ** $P < 0.01$, *** $P < 0.001$. The total number of analyzed
680 oocytes (from 3 independent replicates) is specified above each graph.
681
682 **Supplementary Figure 5:** (A) Quantification of the percentage of unattached kinetochores in
683 oocytes treated with ML141 from Fig. 3B. (B) Schematic depicting the induction of peripheral
684 spindle positioning and treatment with ML141 in oocytes with a centrally positioned nucleus. (C)
685 Quantification of the percentage of unattached kinetochores. (D) Quantification of the average
686 incidence of abnormal K-MT attachment. One-way ANOVA and Tukey's post hoc test were
687 performed to determine statistical significance. Data are displayed as mean ± SEM. Values with

688 asterisks vary significantly, ** P <0.01, *** P <0.001. The total number of analyzed oocytes
689 (from 3 independent replicates) is specified above each graph.
690
691 **Supplementary Figure 6:** (A) Representative images of central and peripheral oocytes treated
692 with or without ML141. The scale bar represents 50 μm. (B,C) Quantification of the relative
693 intensity of F-actin in the cytoplasm and cortex of oocytes, respectively. (D) Representative
694 images of K-MT attachment in prometaphase I oocytes treated with or without ARP2/3 inhibitor,
695 CK-666 at 5 h post *in vitro* maturation. The scale bar represents 10 μm. (E) Quantification of the
696 average incidence of abnormal K-MT attachment in D. One-way ANOVA and Tukey's post hoc
697 test were performed to determine statistical significance. Data are displayed as mean ± SEM.
698 Values with asterisks vary significantly, * P<0.05, ** P<0.01. The total number of analyzed
699 oocytes (from 4 independent replicates) is specified above the graph.
700
701 **Supplementary Figure 7:** Quantification of tyrosinated α-tubulin and α-tubulin intensities in
702 oocytes expressing VASH2/SVBP. One-way ANOVA and Tukey's post hoc test were performed
703 to determine statistical significance. Data are displayed as mean ± SEM. Values with asterisks
704 vary significantly, *** P <0.001. The total number of analyzed oocytes (from 2 independent
705 replicates) is specified above the graph.
706
707 **Supplementary Movie 1:** Time-lapse microscopy of germinal vesicle (GV) oocytes cultured in
708 milrinone-containing medium to maintain prophase I arrest. DIC images were captured every 10
709 minutes at Z-intervals of 5 μm. The scale bar represents 50 μm.
710

713 **REFERENCES**

714 1. H. Sun *et al.*, Global, regional, and national prevalence and disability-adjusted life-years
715 for infertility in 195 countries and territories, 1990-2017: results from a global burden of
716 disease study, 2017. *Aging (Albany NY)* **11**, 10952-10991 (2019).
717 2. P. A. Jacobs, A. G. Baikie, W. M. Court Brown, J. A. Strong, The somatic chromosomes
718 in mongolism. *Lancet* **1**, 710 (1959).
719 3. J. Lejeune, R. Turpin, M. Gautier, [Mongolism; a chromosomal disease (trisomy)]. *Bull*
720 *Acad Natl Med* **143**, 256-265 (1959).
721 4. T. Hassold, P. Hunt, To err (meiotically) is human: the genesis of human aneuploidy. *Nat*
722 *Rev Genet* **2**, 280-291 (2001).
723 5. J. R. Gruhn *et al.*, Chromosome errors in human eggs shape natural fertility over
724 reproductive life span. *Science* **365**, 1466-1469 (2019).
725 6. T. Hassold, H. Hall, P. Hunt, The origin of human aneuploidy: where we have been,
726 where we are going. *Hum Mol Genet* **16 Spec No. 2**, R203-208 (2007).
727 7. H. E. Hall *et al.*, The origin of trisomy 22: evidence for acrocentric chromosome-specific
728 patterns of nondisjunction. *Am J Med Genet A* **143A**, 2249-2255 (2007).
729 8. S. Gilbert, in *Developmental Biology*. (Sinauer Associates, Inc, Sunderland,
730 Massachusetts, 2000), vol. 6th edition.
731 9. S. Brunet, B. Maro, Germinal vesicle position and meiotic maturation in mouse oocyte.
732 *Reproduction* **133**, 1069-1072 (2007).
733 10. M. Almonacid *et al.*, Active diffusion positions the nucleus in mouse oocytes. *Nat Cell*
734 *Biol* **17**, 470-479 (2015).
735 11. M. Almonacid, M. E. Terret, M. H. Verlhac, Control of nucleus positioning in mouse
736 oocytes. *Semin Cell Dev Biol* **82**, 34-40 (2018).
737 12. A. Colin *et al.*, Active diffusion in oocytes nonspecifically centers large objects during
738 prophase I and meiosis I. *J Cell Biol* **219**, (2020).
739 13. M. Almonacid *et al.*, Active Fluctuations of the Nuclear Envelope Shape the
740 Transcriptional Dynamics in Oocytes. *Dev Cell* **51**, 145-157 e110 (2019).
741 14. M. Schuh, J. Ellenberg, Self-organization of MTOCs replaces centrosome function
742 during acentrosomal spindle assembly in live mouse oocytes. *Cell* **130**, 484-498 (2007).
743 15. D. Clift, M. Schuh, A three-step MTOC fragmentation mechanism facilitates bipolar
744 spindle assembly in mouse oocytes. *Nat Commun* **6**, 7217 (2015).
745 16. A. Z. Balboula *et al.*, Haspin kinase regulates microtubule-organizing center clustering
746 and stability through Aurora kinase C in mouse oocytes. *J Cell Sci* **129**, 3648-3660
747 (2016).
748 17. M. Luksza, I. Queguigner, M. H. Verlhac, S. Brunet, Rebuilding MTOCs upon centriole
749 loss during mouse oogenesis. *Dev Biol* **382**, 48-56 (2013).
750 18. E. K. McCarthy, B. Goldstein, Asymmetric spindle positioning. *Curr Opin Cell Biol* **18**,
751 79-85 (2006).
752 19. F. J. Longo, D. Y. Chen, Development of cortical polarity in mouse eggs: involvement of
753 the meiotic apparatus. *Dev Biol* **107**, 382-394 (1985).
754 20. H. Li, F. Guo, B. Rubinstein, R. Li, Actin-driven chromosomal motility leads to
755 symmetry breaking in mammalian meiotic oocytes. *Nat Cell Biol* **10**, 1301-1308 (2008).
756 21. M. H. Verlhac, C. Lefebvre, P. Guillaud, P. Rassinier, B. Maro, Asymmetric division in
757 mouse oocytes: with or without Mos. *Curr Biol* **10**, 1303-1306 (2000).

758 22. M. Schuh, J. Ellenberg, A new model for asymmetric spindle positioning in mouse
759 oocytes. *Curr Biol* **18**, 1986-1992 (2008).
760 23. J. Ma, F. Zeng, R. M. Schultz, H. Tseng, Basonuclin: a novel mammalian maternal-effect
761 gene. *Development* **133**, 2053-2062 (2006).
762 24. Y. J. Menezo, Paternal and maternal factors in preimplantation embryogenesis:
763 interaction with the biochemical environment. *Reprod Biomed Online* **12**, 616-621
764 (2006).
765 25. K. Morohaku *et al.*, Complete in vitro generation of fertile oocytes from mouse
766 primordial germ cells. *Proc Natl Acad Sci U S A* **113**, 9021-9026 (2016).
767 26. J. J. Eppig, M. J. O'Brien, Development in vitro of mouse oocytes from primordial
768 follicles. *Biol Reprod* **54**, 197-207 (1996).
769 27. R. J. Roller, R. A. Kinloch, B. Y. Hiraoka, S. S. Li, P. M. Wassarman, Gene expression
770 during mammalian oogenesis and early embryogenesis: quantification of three messenger
771 RNAs abundant in fully grown mouse oocytes. *Development* **106**, 251-261 (1989).
772 28. A. Inoue, R. Nakajima, M. Nagata, F. Aoki, Contribution of the oocyte nucleus and
773 cytoplasm to the determination of meiotic and developmental competence in mice. *Hum*
774 *Reprod* **23**, 1377-1384 (2008).
775 29. S. I. Lane, Y. Yun, K. T. Jones, Timing of anaphase-promoting complex activation in
776 mouse oocytes is predicted by microtubule-kinetochore attachment but not by bivalent
777 alignment or tension. *Development* **139**, 1947-1955 (2012).
778 30. F. E. Duncan, T. Chiang, R. M. Schultz, M. A. Lampson, Evidence that a defective
779 spindle assembly checkpoint is not the primary cause of maternal age-associated
780 aneuploidy in mouse eggs. *Biol Reprod* **81**, 768-776 (2009).
781 31. A. Z. Balboula, K. Schindler, Selective disruption of aurora C kinase reveals distinct
782 functions from aurora B kinase during meiosis in mouse oocytes. *PLoS Genet* **10**,
783 e1004194 (2014).
784 32. X. Hou *et al.*, Rab6a is a novel regulator of meiotic apparatus and maturational
785 progression in mouse oocytes. *Sci Rep* **6**, 22209 (2016).
786 33. I. Bennabi *et al.*, Artificially decreasing cortical tension generates aneuploidy in mouse
787 oocytes. *Nat Commun* **11**, 1649 (2020).
788 34. A. Z. Balboula, K. Schindler, T. Kotani, M. Kawahara, M. Takahashi, Vitrification-
789 induced activation of lysosomal cathepsin B perturbs spindle assembly checkpoint
790 function in mouse oocytes. *Mol Hum Reprod* **26**, 689-701 (2020).
791 35. S. I. Lane, H. Y. Chang, P. C. Jennings, K. T. Jones, The Aurora kinase inhibitor
792 ZM447439 accelerates first meiosis in mouse oocytes by overriding the spindle assembly
793 checkpoint. *Reproduction* **140**, 521-530 (2010).
794 36. T. Akera *et al.*, Spindle asymmetry drives non-Mendelian chromosome segregation.
795 *Science* **358**, 668-672 (2017).
796 37. J. Sebestova, A. Danylevska, L. Novakova, M. Kubelka, M. Anger, Lack of response to
797 unaligned chromosomes in mammalian female gametes. *Cell Cycle* **11**, 3011-3018
798 (2012).
799 38. C. L. Rieder, The structure of the cold-stable kinetochore fiber in metaphase PtK1 cells.
800 *Chromosoma* **84**, 145-158 (1981).
801 39. A. Sanfins, G. Y. Lee, C. E. Plancha, E. W. Overstrom, D. F. Albertini, Distinctions in
802 meiotic spindle structure and assembly during in vitro and in vivo maturation of mouse
803 oocytes. *Biol Reprod* **69**, 2059-2067 (2003).

804 40. A. Sanfins, C. E. Plancha, E. W. Overstrom, D. F. Albertini, Meiotic spindle
805 morphogenesis in in vivo and in vitro matured mouse oocytes: insights into the
806 relationship between nuclear and cytoplasmic quality. *Hum Reprod* **19**, 2889-2899
807 (2004).
808 41. B. G. Tatham *et al.*, Centrifugation of bovine oocytes for nuclear micromanipulation and
809 sperm microinjection. *Hum Reprod* **11**, 1499-1503 (1996).
810 42. A. Metchat *et al.*, An actin-dependent spindle position checkpoint ensures the asymmetric
811 division in mouse oocytes. *Nat Commun* **6**, 7784 (retracted) (2015).
812 43. A. Ferrieres *et al.*, Oocyte recovery post human follicular fluid centrifugation in modified
813 natural cycle and achieving embryo. *Reprod Biomed Online* **18**, 671-673 (2009).
814 44. J. T. Chung, B. R. Downey, R. F. Casper, R. C. Chian, Effect of centrifugation on early
815 embryonic development and parthenogenetic activation of bovine oocytes matured in
816 vitro. *Reprod Fertil Dev* **13**, 383-388 (2001).
817 45. K. Hara *et al.*, Extrusion and removal of lipid from the cytoplasm of porcine oocytes at
818 the germinal vesicle stage: centrifugation under hypertonic conditions influences
819 vitrification. *Cryobiology* **50**, 216-222 (2005).
820 46. T. S. Kitajima, M. Ohsugi, J. Ellenberg, Complete kinetochore tracking reveals error-
821 prone homologous chromosome biorientation in mammalian oocytes. *Cell* **146**, 568-581
822 (2011).
823 47. H. Yan *et al.*, CDC42 controls the activation of primordial follicles by regulating PI3K
824 signaling in mouse oocytes. *BMC Biol* **16**, 73 (2018).
825 48. Y. Zhang *et al.*, The small GTPase CDC42 regulates actin dynamics during porcine
826 oocyte maturation. *J Reprod Dev* **63**, 505-510 (2017).
827 49. Z. Surviladze *et al.*, in *Probe Reports from the NIH Molecular Libraries Program*.
828 (Bethesda (MD), 2010).
829 50. B. Dehapiot, V. Carriere, J. Carroll, G. Halet, Polarized Cdc42 activation promotes polar
830 body protrusion and asymmetric division in mouse oocytes. *Dev Biol* **377**, 202-212
831 (2013).
832 51. K. Yi *et al.*, Dynamic maintenance of asymmetric meiotic spindle position through
833 Arp2/3-complex-driven cytoplasmic streaming in mouse oocytes. *Nat Cell Biol* **13**, 1252-
834 1258 (2011).
835 52. B. J. Nolen *et al.*, Characterization of two classes of small molecule inhibitors of Arp2/3
836 complex. *Nature* **460**, 1031-1034 (2009).
837 53. J. C. Bulinski, J. E. Richards, G. Piperno, Posttranslational modifications of alpha
838 tubulin: detyrosination and acetylation differentiate populations of interphase
839 microtubules in cultured cells. *J Cell Biol* **106**, 1213-1220 (1988).
840 54. L. T. Ferreira *et al.*, alpha-Tubulin detyrosination impairs mitotic error correction by
841 suppressing MCAK centromeric activity. *J Cell Biol* **219**, (2020).
842 55. J. Nieuwenhuis *et al.*, Vasohibins encode tubulin detyrosinating activity. *Science* **358**,
843 1453-1456 (2017).
844 56. C. Aillaud *et al.*, Vasohibins/SVBP are tubulin carboxypeptidases (TCPs) that regulate
845 neuron differentiation. *Science* **358**, 1448-1453 (2017).
846 57. B. Mogessie, M. Schuh, Actin protects mammalian eggs against chromosome segregation
847 errors. *Science* **357**, (2017).

848 58. S. L. Barrett, D. F. Albertini, Cumulus cell contact during oocyte maturation in mice
849 regulates meiotic spindle positioning and enhances developmental competence. *J Assist*
850 *Reprod Genet* **27**, 29-39 (2010).
851 59. M. Levi, Y. Ghetler, A. Shulman, R. Shalgi, Morphological and molecular markers are
852 correlated with maturation-competence of human oocytes. *Hum Reprod* **28**, 2482-2489
853 (2013).
854 60. A. Gonzalez-Reyes, H. Elliott, D. St Johnston, Polarization of both major body axes in
855 Drosophila by gurken-torpedo signalling. *Nature* **375**, 654-658 (1995).
856 61. S. Roth, F. S. Neuman-Silberberg, G. Barcelo, T. Schupbach, cornichon and the EGF
857 receptor signaling process are necessary for both anterior-posterior and dorsal-ventral
858 pattern formation in Drosophila. *Cell* **81**, 967-978 (1995).
859 62. T. Zhao, O. S. Graham, A. Raposo, D. St Johnston, Growing microtubules push the
860 oocyte nucleus to polarize the Drosophila dorsal-ventral axis. *Science* **336**, 999-1003
861 (2012).
862 63. S. W. Grill, J. Howard, E. Schaffer, E. H. Stelzer, A. A. Hyman, The distribution of
863 active force generators controls mitotic spindle position. *Science* **301**, 518-521 (2003).
864 64. D. G. Albertson, Formation of the first cleavage spindle in nematode embryos. *Dev Biol*
865 **101**, 61-72 (1984).
866 65. S. W. Grill, P. Gonczy, E. H. Stelzer, A. A. Hyman, Polarity controls forces governing
867 asymmetric spindle positioning in the Caenorhabditis elegans embryo. *Nature* **409**, 630-
868 633 (2001).
869 66. M. B. Goulding, J. C. Canman, E. N. Senning, A. H. Marcus, B. Bowerman, Control of
870 nuclear centration in the C. elegans zygote by receptor-independent Galpha signaling and
871 myosin II. *J Cell Biol* **178**, 1177-1191 (2007).
872 67. G. Nargund *et al.*, Cumulative conception and live birth rates in natural (unstimulated)
873 IVF cycles. *Hum Reprod* **16**, 259-262 (2001).
874 68. S. f. A. R. Technology. (2019).
875 69. D. Londono-Vasquez, K. Rodriguez-Lukey, S. K. Behura, A. Z. Balboula, Microtubule
876 organizing centers regulate spindle positioning in mouse oocytes. *Dev Cell* **57**, 197-211
877 e193 (2022).
878 70. P. Stein, K. Schindler, Mouse oocyte microinjection, maturation and ploidy assessment. *J*
879 *Vis Exp*, (2011).
880 71. C. L. Chatot, C. A. Ziomek, B. D. Bavister, J. L. Lewis, I. Torres, An improved culture
881 medium supports development of random-bred 1-cell mouse embryos in vitro. *J Reprod*
882 *Fertil* **86**, 679-688 (1989).

883

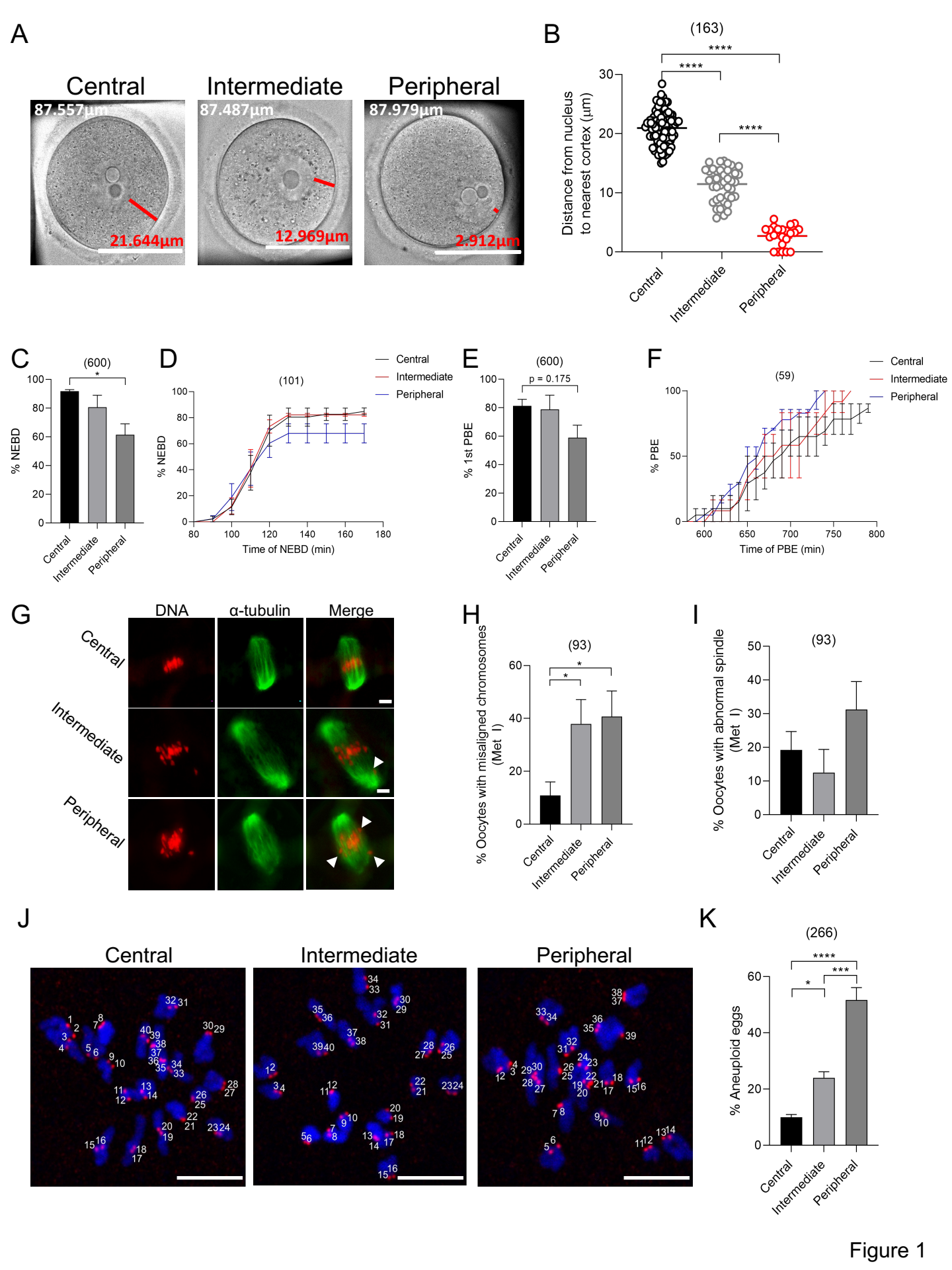
A
Central
Intermediate
Peripheral
87.557µm
21.644µm
87.487µm
12.969µm
87.979µm
2.912µm
B
(163)
****
****
****
Distance from nucleus to nearest cortex (µm)
Central
Intermediate
Peripheral
C
(600)
*
% NEBD
Central
Intermediate
Peripheral
D
(101)
Central
Intermediate
Peripheral
% NEBD
Time of NEBD (min)
E
(600)
p = 0.175
% 1st PBE
Central
Intermediate
Peripheral
F
(59)
Central
Intermediate
Peripheral
% PBE
Time of PBE (min)
G
DNA
α-tubulin
Merge
Central
Intermediate
Peripheral
H
(93)
*
*
% Oocytes with misaligned chromosomes (Met I)
Central
Intermediate
Peripheral
I
(93)
% Oocytes with abnormal spindle (Met I)
Central
Intermediate
Peripheral
J
Central
Intermediate
Peripheral
K
(266)
****
***
*
% Aneuploid eggs
Central
Intermediate
Peripheral

Figure 1

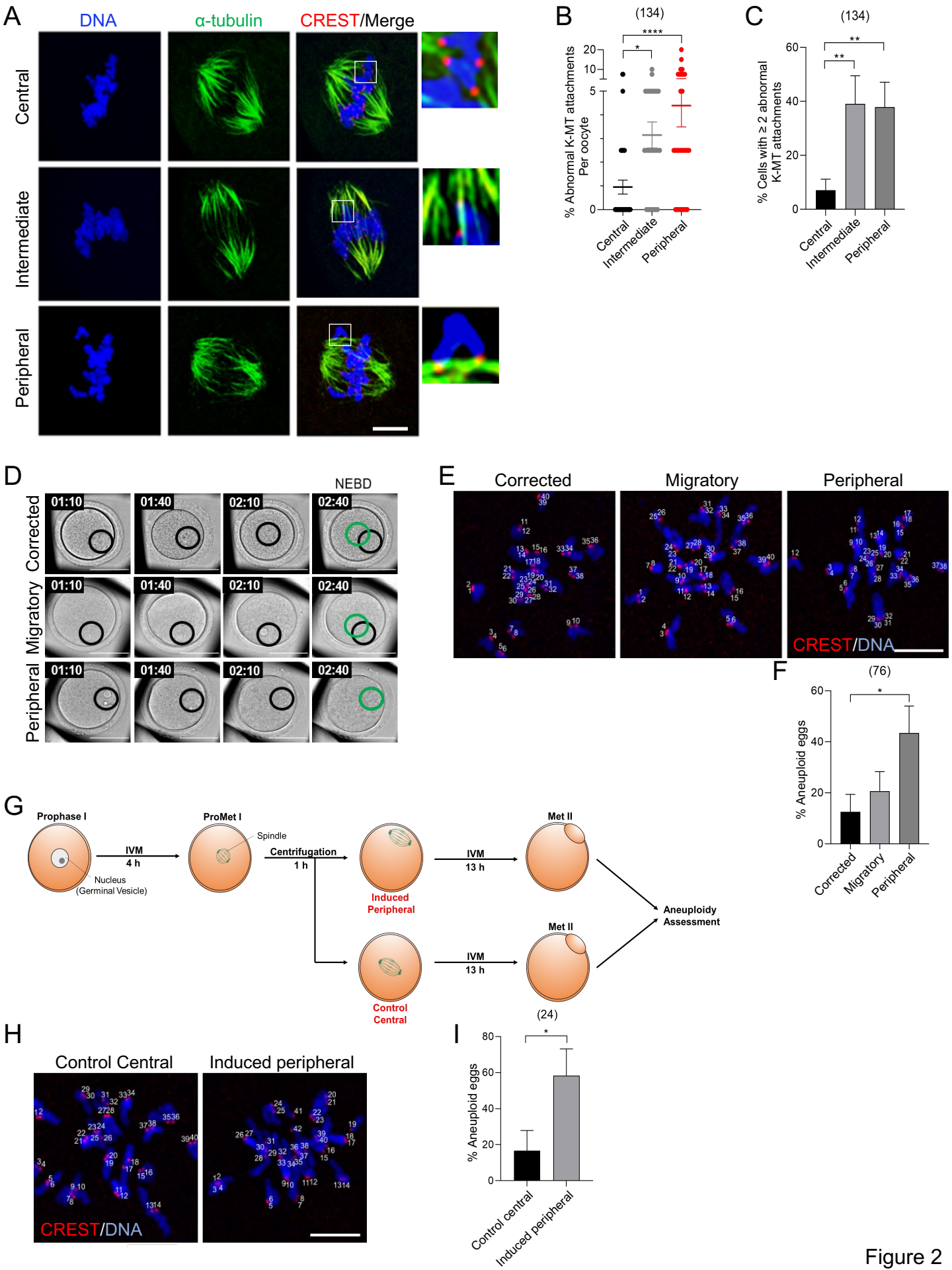
A
DNA
α-tubulin
CREST/Merge
Central
Intermediate
Peripheral
B
(134)
% Abnormal K-MT attachments Per oocyte
Central
Intermediate
Peripheral
C
(134)
% Cells with ≥ 2 abnormal K-MT attachments
Central
Intermediate
Peripheral
D
NEBD
Corrected
Migratory
Peripheral
01:10
01:40
02:10
02:40
E
Corrected
Migratory
Peripheral
CREST/DNA
F
(76)
% Aneuploid eggs
Corrected
Migratory
Peripheral
G
Prophase I
Nucleus (Germinal Vesicle)
IVM 4 h
ProMet I
Spindle
Centrifugation 1 h
Induced Peripheral
Control Central
IVM 13 h
Met II
Aneuploidy Assessment
H
Control Central
Induced peripheral
CREST/DNA
I
(24)
% Aneuploid eggs
Control central
Induced peripheral

Figure 2

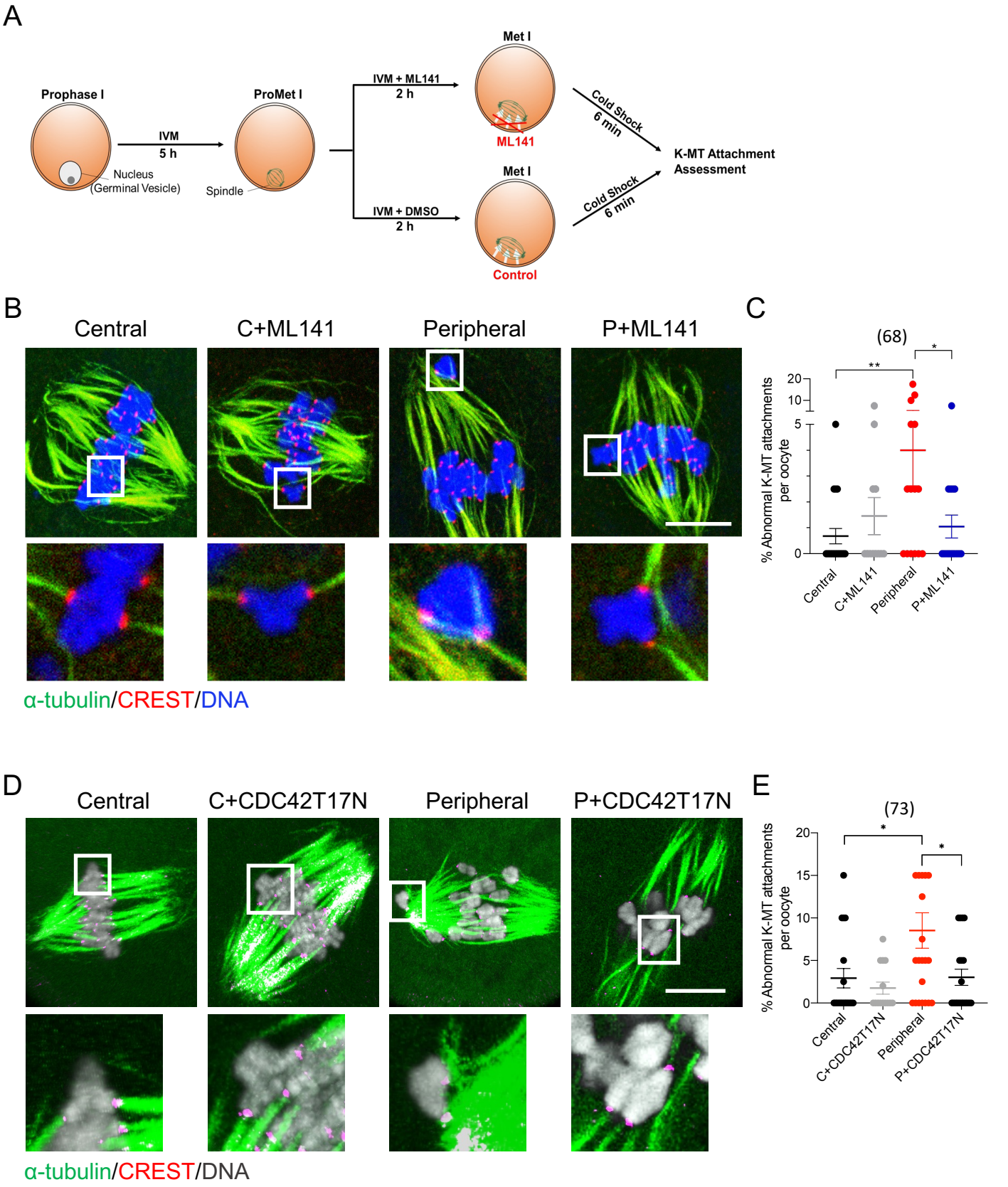
A
Prophase I
IVM
5 h
Nucleus
(Germinal Vesicle)
ProMet I
Spindle
IVM + ML141
2 h
Met I
ML141
IVM + DMSO
2 h
Met I
Control
Cold Shock
6 min
Cold Shock
6 min
K-MT Attachment
Assessment
B
Central
C+ML141
Peripheral
P+ML141
α-tubulin/CREST/DNA
C
(68)
% Abnormal K-MT attachments
per oocyte
Central
C+ML141
Peripheral
P+ML141
D
Central
C+CDC42T17N
Peripheral
P+CDC42T17N
α-tubulin/CREST/DNA
E
(73)
% Abnormal K-MT attachments
per oocyte
Central
C+CDC42T17N
Peripheral
P+CDC42T17N

Figure 3

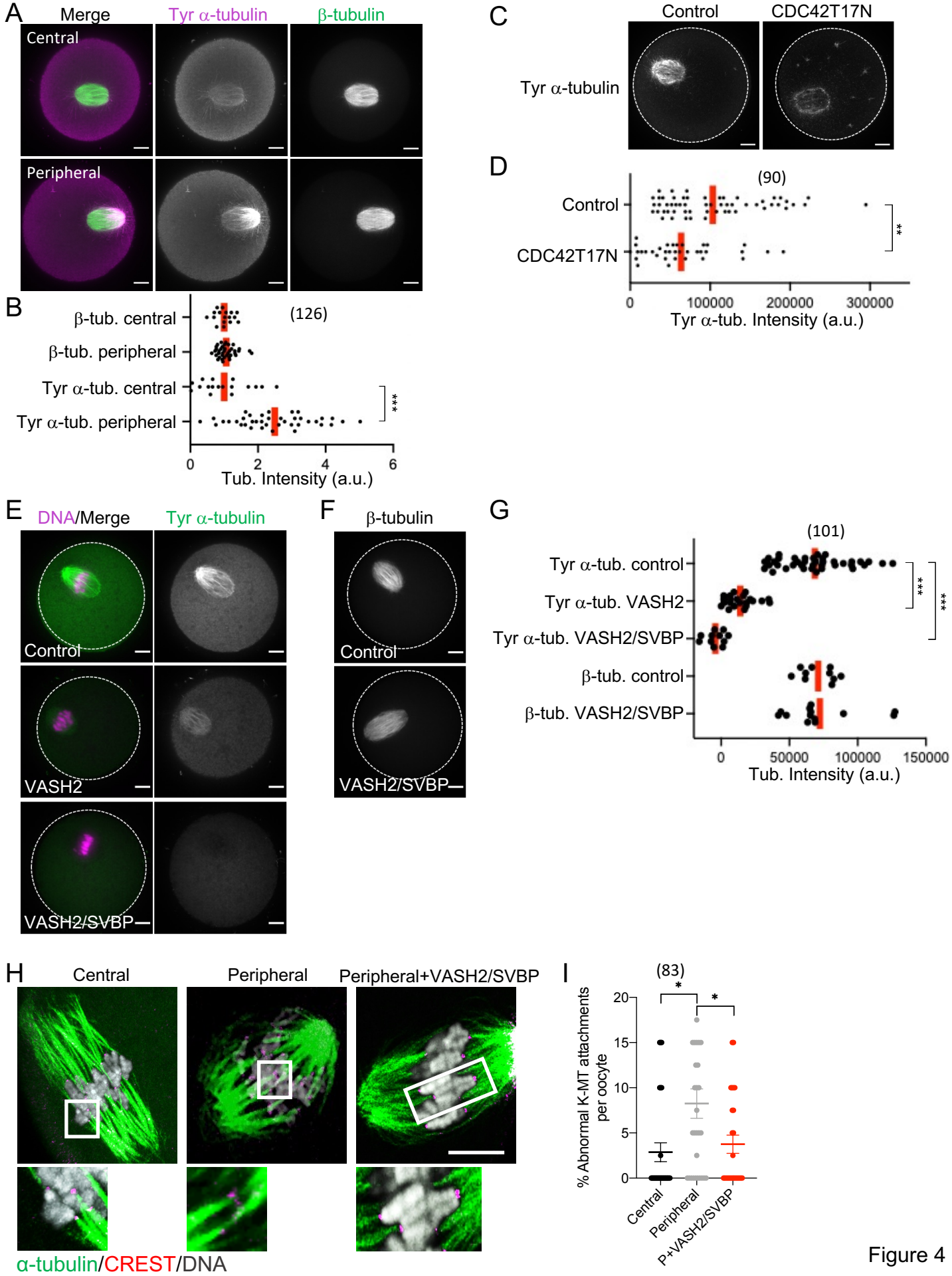
A
Merge
Tyr α-tubulin
β-tubulin
Central
Peripheral
B
β-tub. central
β-tub. peripheral
Tyr α-tub. central
Tyr α-tub. peripheral
(126)
***
0
2
4
6
Tub. Intensity (a.u.)
C
Control
CDC42T17N
Tyr α-tubulin
D
(90)
Control
CDC42T17N
**
0
100000
200000
300000
Tyr α-tub. Intensity (a.u.)
E
DNA/Merge
Tyr α-tubulin
Control
VASH2
VASH2/SVBP
F
β-tubulin
Control
VASH2/SVBP
G
(101)
Tyr α-tub. control
Tyr α-tub. VASH2
Tyr α-tub. VASH2/SVBP
β-tub. control
β-tub. VASH2/SVBP
***
***
0
50000
100000
150000
Tub. Intensity (a.u.)
H
Central
Peripheral
Peripheral+VASH2/SVBP
α-tubulin/CREST/DNA
I
(83)
*
*
% Abnormal K-MT attachments per oocyte
20
15
10
5
0
Central
Peripheral
P+VASH2/SVBP

Figure 4

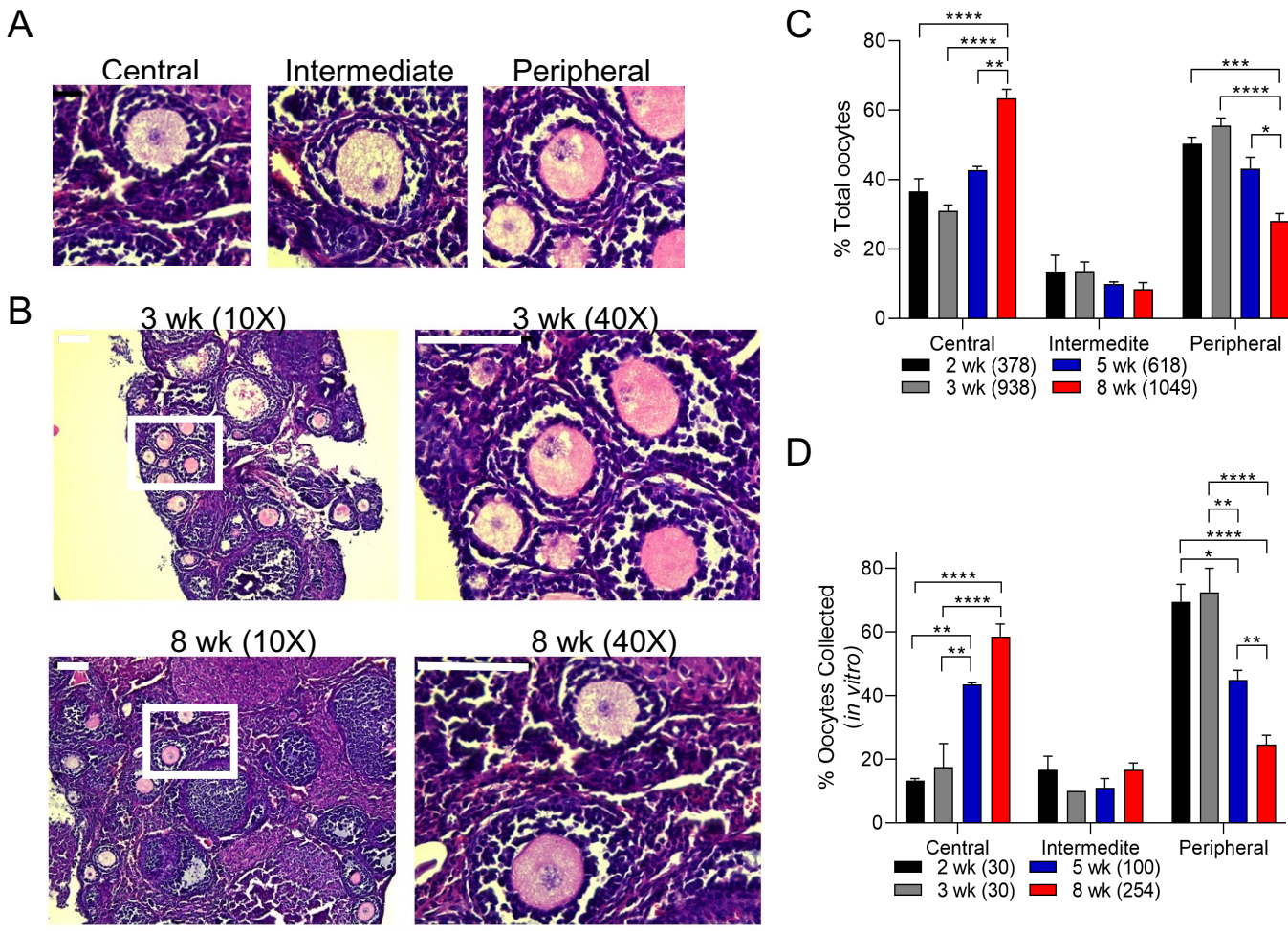
A
Central
Intermediate
Peripheral
B
3 wk (10X)
3 wk (40X)
8 wk (10X)
8 wk (40X)
C
% Total oocytes
0
20
40
60
80
****
****
**
***
****
*
Central
Intermedite
Peripheral
2 wk (378)
3 wk (938)
5 wk (618)
8 wk (1049)
D
% Oocytes Collected
(in vitro)
0
20
40
60
80
****
****
**
**
****
**
****
*
**
Central
Intermedite
Peripheral
2 wk (30)
3 wk (30)
5 wk (100)
8 wk (254)

Figure 5

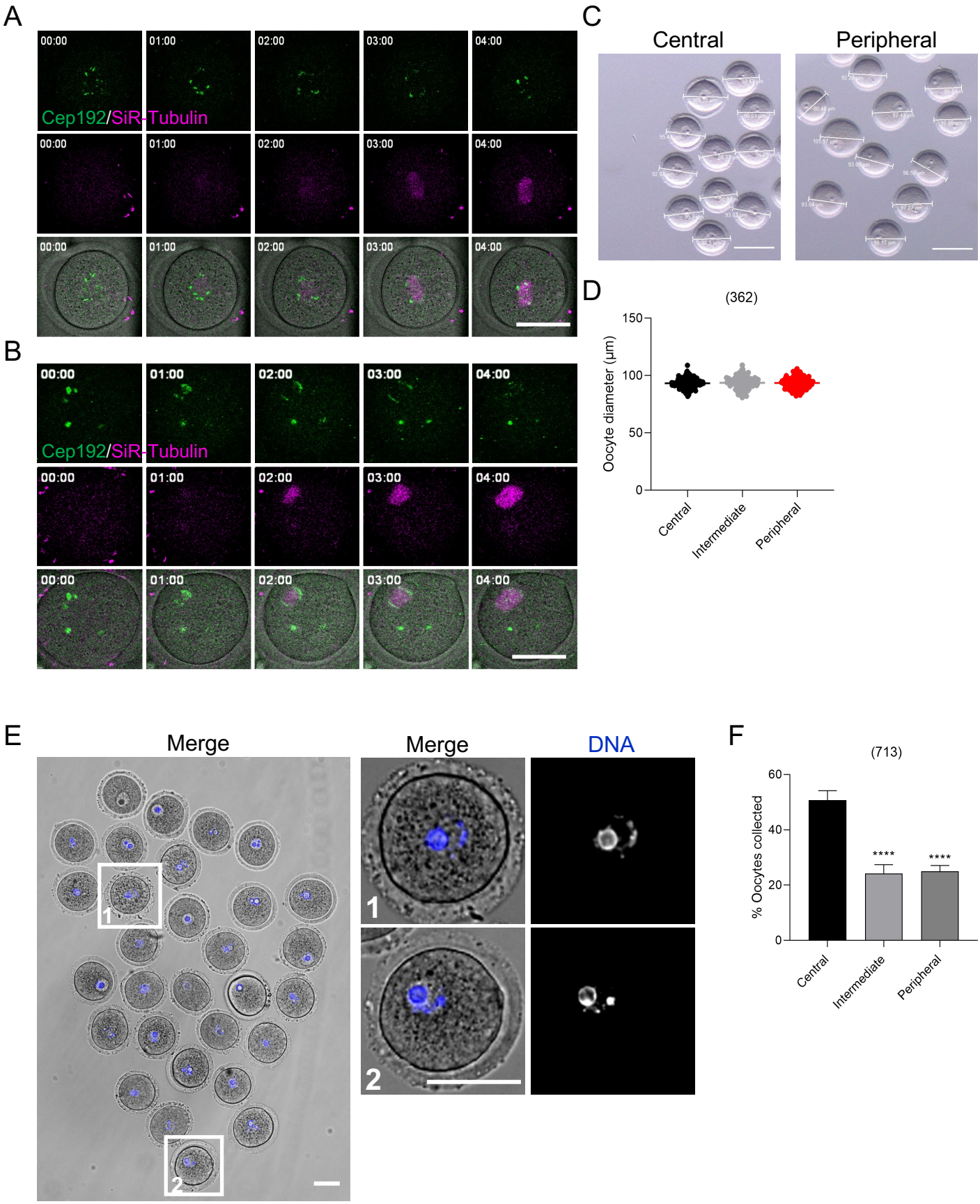

Supplementary Figure 1

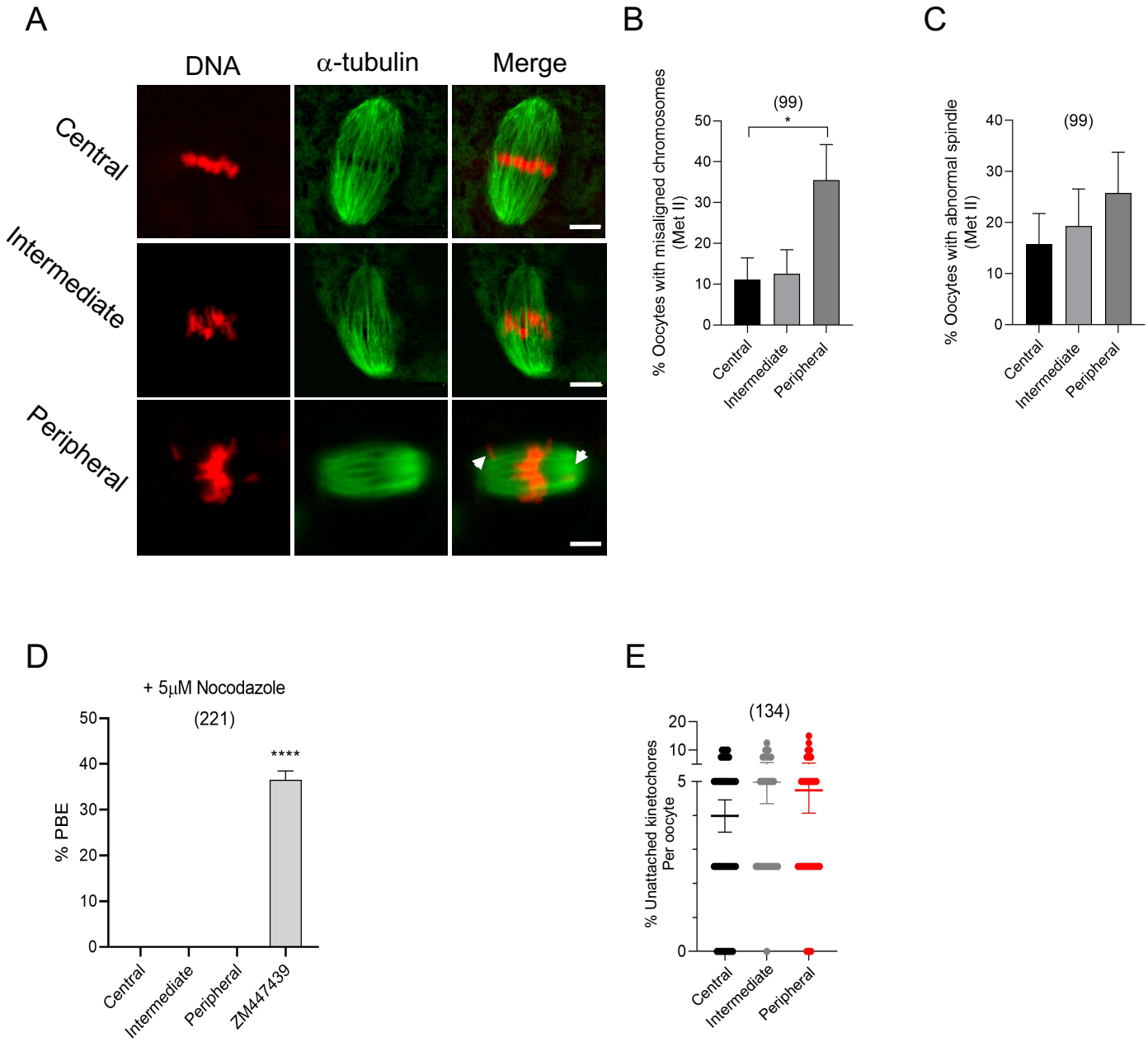

Supplementary Figure 2

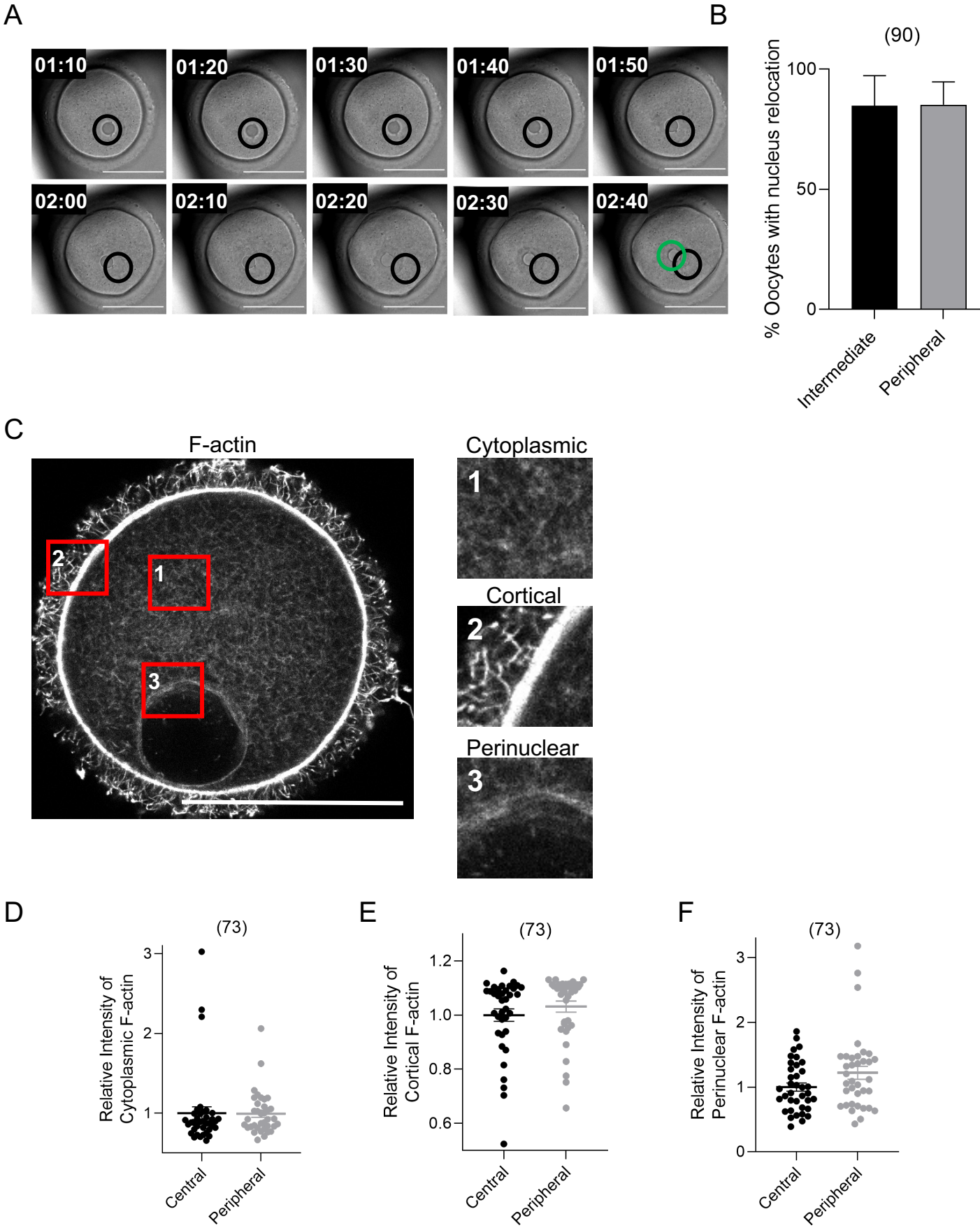

Supplementary Figure 3

A

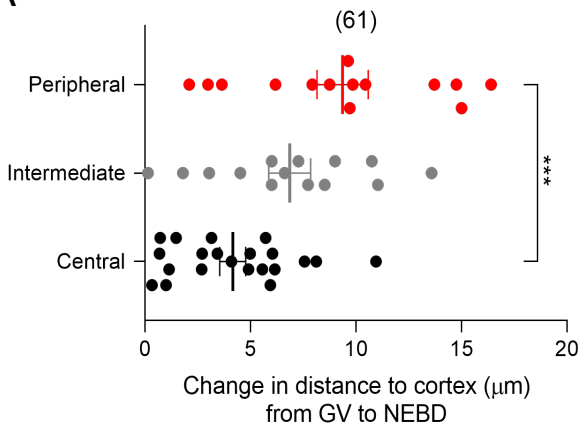

B

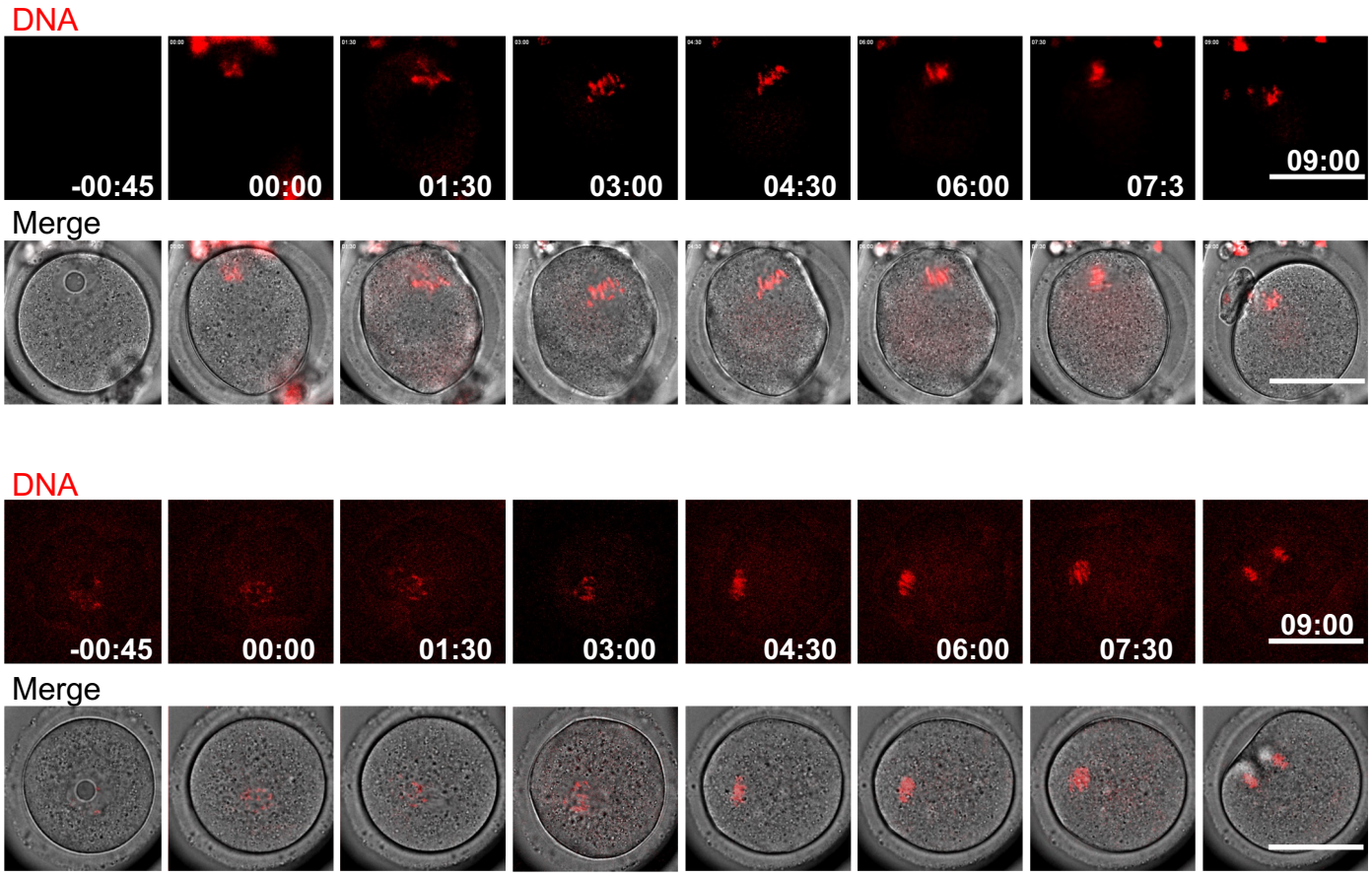

C

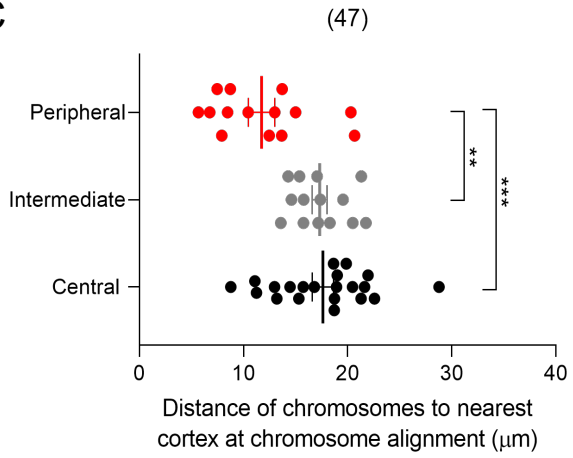

D

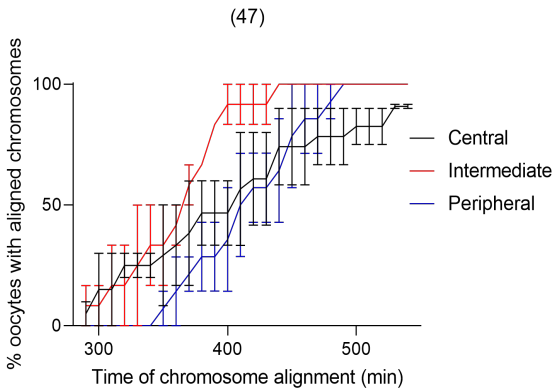

Supplementary Figure 4

A

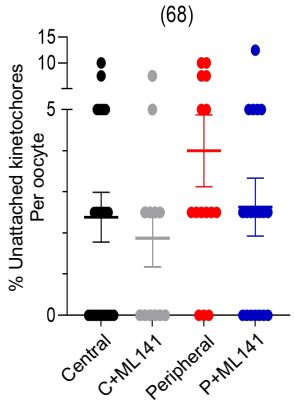

B

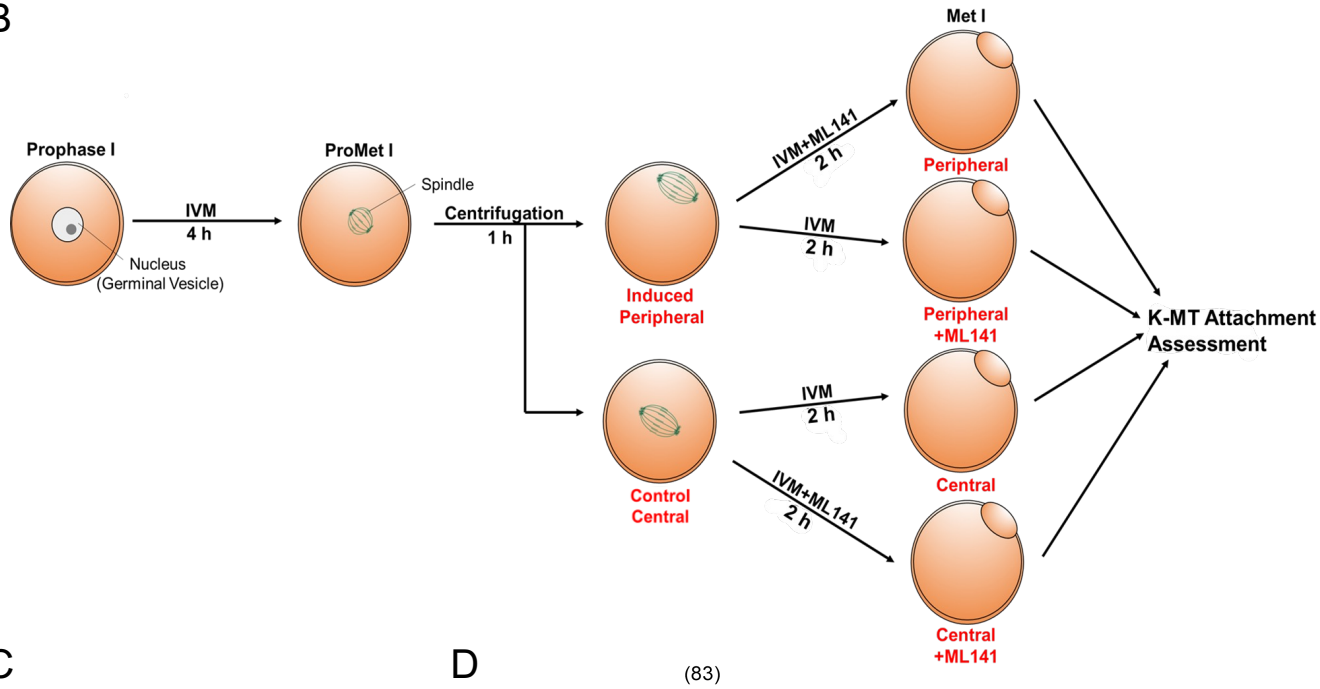

C

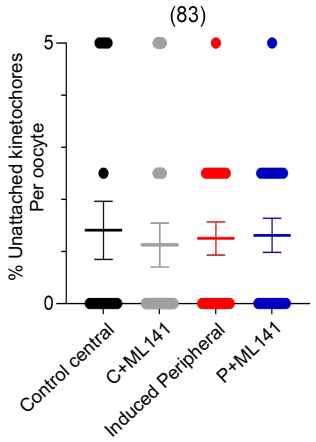

D

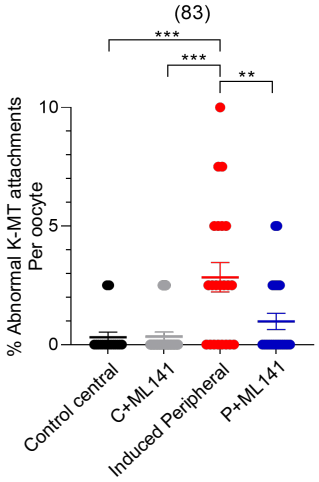

Supplementary Figure 5

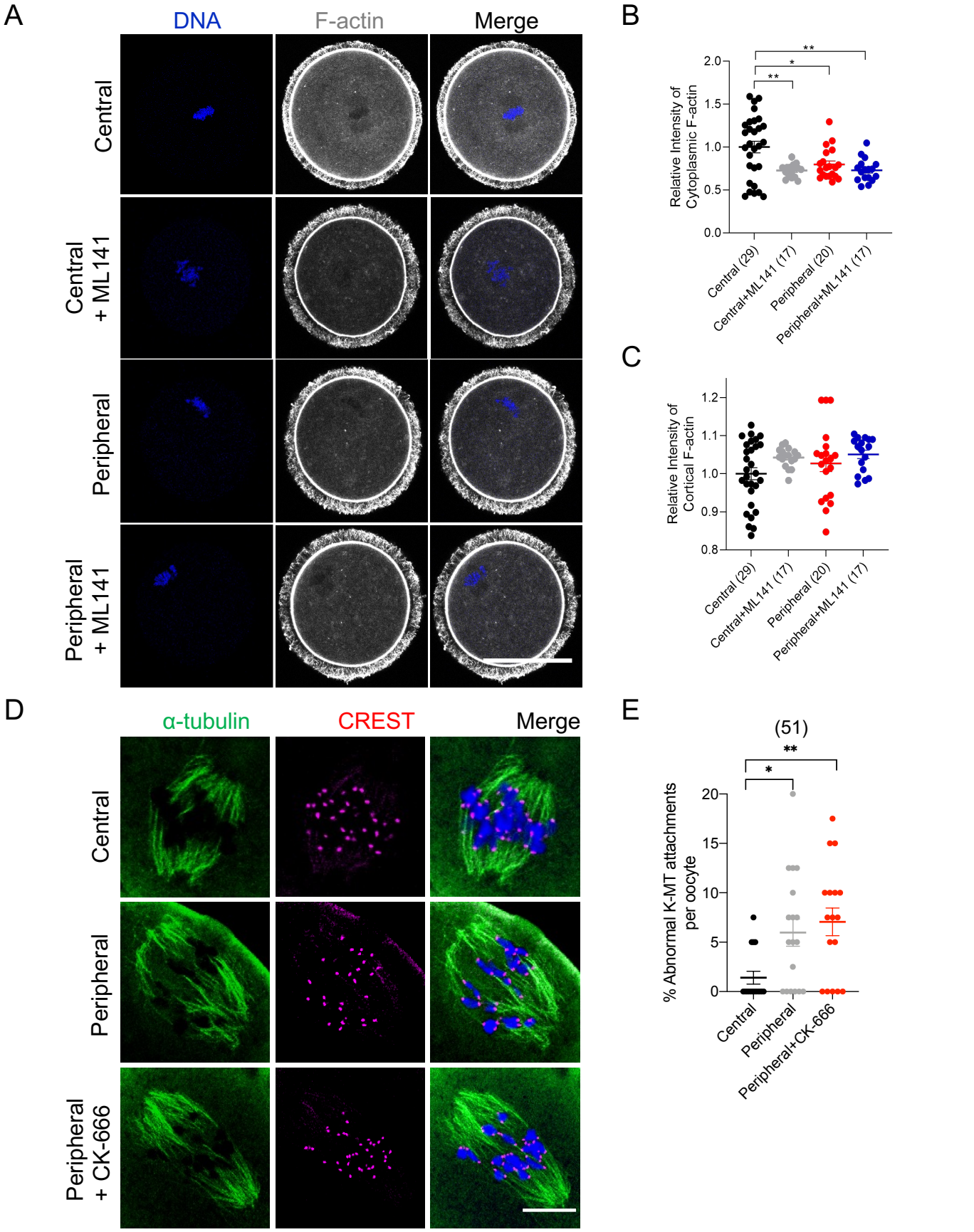

Supplementary Figure 6

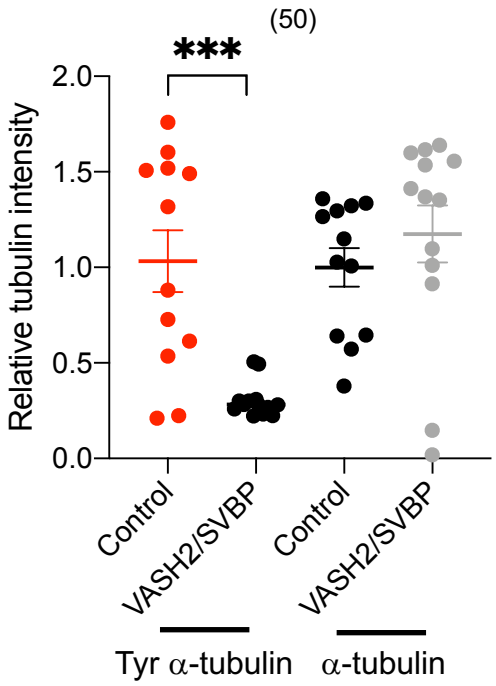

Supplementary Figure 7